NATIONAL UNIVERSITY OF SCIENCE AND TECHNOLOGY
POLITEHNICA BUCHAREST
FACULTY OF CHEMICAL ENGINEERING AND BIOTECHNOLOGIES
DEPARTMENT OF GENERAL CHEMISTRY

ABSTRACT

DOCTORAL THESIS

Doctoral Supervisors:
Prof. Dr. Ioana DEMETRESCU
Prof. Dr. Doina DRĂGĂNESCU

Author:
Eng. Manuela-Elena VOICU

Bucharest
2023

NATIONAL UNIVERSITY OF SCIENCE AND TECHNOLOGY
POLITEHNICA BUCHAREST
FACULTY OF CHEMICAL ENGINEERING AND BIOTECHNOLOGIES
DEPARTMENT OF GENERAL CHEMISTRY

DOCTORAL THESIS – ENGLISH ABSTRACT

INTERFACES IN THE DEVELOPMENT AND CHARACTERIZATION OF BIODEGRADABLE AND NON BIODEGRADABLE METAL ALLOY

Doctoral Supervisors:
Prof. Dr. Ioana DEMETRESCU
Prof. Dr. Doina DRĂGĂNESCU

Author:
Eng. Manuela-Elena VOICU

Bucharest
2023

ABSTRACT
INTERFACES IN THE DEVELOPMENT AND CHARACTERIZATION OF BIODEGRADABLE AND NON BIODEGRADABLE METAL ALLOY

Keywords: biodegradable alloy AZ31; TiZr alloy; polylactic acid; electrospinning; dip-coating; NADES; electrochemical stability; drug encapsulation; antibacterial effect; morphological characterizations

The abstract of the Ph.D. thesis briefly includes the content of the bibliographic research (Chapters I-III) and original research (Chapters IV-IX). The numbering of chapters, sub-chapters, figures, and tables correspond to those in the thesis. A selective bibliography and a list of publications are also included at the end of this summary.

Eng. Manuela-Elena VOICU

ABSTRACT

INTERFACES IN THE DEVELOPMENT AND CHARACTERIZATION OF BIODEGRADABLE AND NON BIODEGRADABLE METAL ALLOY

TABLE OF CONTENTS

INTRODUCTION

Metallic materials are widely used in medical applications because of their ability to osseointegrate, biocompatibility, and corrosion resistance.

On the other side, biodegradable metal materials used as temporary implants, such as screws, plates, wires, or for bone fixation are useful to avoid secondary surgery.

For better biocompatibility, antibacterial activity, adhesion, and cell proliferation, coatings can be used on both biodegradable and non-biodegradable alloy surfaces. Coatings can serve as drug encapsulation structures and lead to controlled drug release.

Given that bacteria are aggressive, leading to dangerous infections and even implant rejection, drug-encapsulated materials are the ideal solution.

Therefore, the research supporting the present Ph.D. thesis includes different coating procedures on biodegradable and non-biodegradable metal substrates and their characterizations, including microstructure, electrochemical stability, adhesion, encapsulation-drug release, and antibacterial activity.

The principal objective of the Ph.D. thesis is to investigate the potential of new biodegradable (AZ31 alloy) and non-biodegradable (TiZr alloy) materials with polymer coatings to provide structures for controlled drug release.

The first part of this Ph.D. thesis, *bibliographical research*, contains three chapters representing generalities about materials and their characterizations.

Chapter I includes literature data on current trends in biodegradable and non-biodegradable metallic biomaterials. Also, to improve the characteristics of alloys, biocompatibility, and antibacterial activity, their surfaces can be physically and chemically modified.

Chapter II discusses aspects of drug encapsulation in structures deposited on the alloys studied in this thesis.

Chapter III focuses on the most important experimental methods for obtaining and characterized uncoated and coated alloys, such as electrochemical methods, morphological and functional characterizations.

The second part of the Ph.D. thesis, *original research*, contains chapters IV-IX, which include the results of the original experimental research, their processing, and interpretation, conclusions, as well as bibliographical sources, and a list of publications.

Chapter IV contains the biodegradable and non-biodegradable materials used as substrates in the experiments, the surface preparation of the substrates, and the solutions and equipment used for the electrochemical and physicochemical characterizations of the coatings.

Chapters V and *VI* present surface modifications of AZ31 biodegradable alloy by coating with PLA and their characterization using FT-IR, SEM, contact angle, ICP-MS, BET analysis, and adhesion force analysis.

Chapter VII presents the surface modification of the non-biodegradable TiZr alloy by coating it with different polymers. First, PLA nanofibers are deposited by electrospinning technique, and the second coating of the alloy consists of polypyrrole deposition concomitant with gentamicin encapsulation by electropolymerization, studied for the first time in the literature. Both coatings were characterized by FT-IR,

contact angle, and SEM analyses, and the polypyrrole coating with gentamicin was subjected to drug release tests and determination of antibacterial activity.

Chapters VIII and *IX* contain electrochemical characterizations of PLA coatings, as well as encapsulation-release of gentamicin and antibacterial effects on biodegradable and non-biodegradable materials.

The thesis concludes with Final Conclusions containing the original contributions.

CHAPTER I

CURRENT TRENDS IN METALLIC BIOMATERIALS RESEARCH

In terms of materials used as implants, there are three types: metallic materials, ceramic materials, and polymeric materials [6].

Metallic biomaterials are the most widely used for medical applications, accounting for about 70% of implants, due to their superior mechanical properties, good durability, and high biocompatibility [8, 9].

Metallic materials are used in many applications, predominantly in orthopedic surgery as bone plates, screws, bolts, and in joint replacement, making them more advantageous than polymeric and ceramic materials [15].

The need to use implants with properties closer to those of human bone has led to the alloying of Ti, resulting various alloys of Ti [20].

Alloying Ti with various metals such as zirconium (Zr), which exhibits good tissue biocompatibility, high mechanical strength, and corrosion resistance [21], can be used as implants in orthopedic and dental surgery. These metals, Ti and Zr, are corrosion-resistant metals in many aggressive environments, including bio-liquids due to the existence of a native passive layer integrated into tissues [26].

In addition to the metals most commonly used in permanent implants, biodegradable metals have been developed as ideal materials for temporary implants. They safely degrade in the human body after they have fulfilled their function, thus avoiding a new operation to remove the implant, speeding up the healing process, reducing the risks of a permanent implant, and ultimately reducing time and costs hospitalization [29].

Magnesium alloys are light, have high specific strength, have good corrosion resistance, and are easy to cast. Magnesium is considered an ideal material for implantable devices in the medical industry because it is light and strong. Also, has a similar density to human bone and is non-toxic, his corrosion in the body takes place over several weeks to months, during this time, the stability of the implant is ensured until it is completely dissolved and the tissue healing process is complete [31-34].

Surface modification of an alloy used as an implant plays an important role, significantly improving the biocompatibility and antibacterial activity of the implant [42], increasing implant integrity and tissue adhesion, and avoids implant rejection by the body or inflammatory reactions [22]. Usually, after implantation, a metal implant is surrounded by fibrous tissue, which prevents bioactive interaction between the implant and the host tissue [43].

Currently, controlling and monitoring the biodegradation rates of Mg alloys after surface modifications by various procedures is one of the important challenges in implant research [49, 50].

CHAPTER II

ENCAPSULATION AND RELEASE OF DRUG ON THE SURFACE OF ALLOYS

The most common problems after surgery include implant infections, and the most useful strategy is the use of various drugs that can be encapsulated in the implant for controlled release [67].

Drug release from biodegradable polymer coatings depends on encapsulation efficiency, solubility, diffusion, the size of the coating structure, and biodegradability [68].

To prevent post-operative inflammation after the insertion of an implant, anti-inflammatory drugs can be used preventive or immediately post-operative. These can be taken orally or can be encapsulated in various forms in the implanted material, either in the oral cavity [70] or in orthopedics.

Bacterial infections and inflammation are frequently present after surgery, therefore several drugs are administered for protection. Drugs are usually administered orally, but with the development of nanotechnology, new approaches have been developed, such as delivering drugs directly from implants with numerous benefits including the ability to increase the efficiency of administration of therapeutic agents in terms of both loading and controlled release as part of improving their bioactive potential [72].

The encapsulation and release kinetics of several known antibiotics used to improve the antibacterial effect have been studied over time. The synergistic effect of nanoscale drug delivery is noted for the use of different forms of nano-sized coatings because different coatings can provide a high surface-to-volume ratio, surface functionality, and increased antibacterial effect [72-74]. In some applications, the drug encapsulated in the implant has a beneficial effect on the biocompatibility and stability of the implant, providing it with a multifunctional that has been investigated, for example, for the encapsulation of cysteine, a drug with a characteristic zwitterionic structure [75].

The most frequently identified bacteria causing infections are gram-negative and gram-positive microorganisms, specifically Staphylococcus aureus (39.28%) and Escherichia coli (30.35%) [76].

Gentamicin sulfate is an aminoglycoside, bactericidal, heat-stable antibiotic used as a prophylactic in orthopedic surgery or in various treatments for bone infections with gram-positive or gram-negative microorganisms [76].

Encapsulation of the drug in polylactic acid nanofibres improves the action of the drug through controlled and sustained release directly at the site of action. Antibiotics are used to improve efficacy and prevent the growth of bacteria resistant to antibiotics [66].

CHAPTER IV

MATERIALS AND METHODS

For the experiments in this Ph.D. thesis, the biodegradable MgAlZn alloy (AZ31) with 96:3:1 wt% molar ratio, was cut in samples with dimensions of 2×2 cm and 1 mm thickness.

The non-biodegradable material used was TiZr (50:50 wt%), samples with dimensions of 2×2 cm and 2 mm thickness.

All alloy samples have been previously prepared by grinding and cleaning.

TiZr alloy samples were exposed to an acid pretreatment ($3HNO_3$:1HF:$2H_2O$) known as *"etching"*.

Surface modification of AZ31 alloy and TiZr alloy with PLA coating was performed using a solution prepared by dissolving PLA granules in a mixture of chloroform ($CHCl_3$) and N,N-dimethylformamide (DMF) (ratio 1:1.5 v/v).

The non-biodegradable TiZr alloy was coated with pyrrole (Py) by electropolymerization from ionic liquids based on choline chloride (ChCl) and lactic acid (LA) in a molar ratio of 1:2 (ChCl:LA). 0.5M Py was added to the obtained solution and 50mM gentamicin sulphate (GS) was encapsulated under magnetic stirring.

Also, gentamicin sulphate was used as a drug for encapsulation in polymer coatings and was prepared in phosphate buffer saline (PBS) of various pHs. The concentration of GS in the encapsulation was 2 g/L.

The techniques used for polymer coatings were as follows:

- *Electrospinning technique* was used to deposit PLA nanofibers on AZ31 and TiZr alloy surfaces.

- *Dip-coating technique (immersion technique)* was used for coating the alloy AZ31 with PLA by dipping the AZ31 alloy sample in PLA solution. Samples obtained by this technique are further described as *"dip"*.

- *Electropolymerization* of PPy and PPy-GS by ionic liquids (NADES - *Natural Deep Eutectic Solvents*) included the use of electrochemical methods such as cyclic voltammetry and chronoamperometry using an AutoLab40 potentiostat-galvanostat and an electrochemical cell consisting of a reference electrode, an Ag wire, the working electrode, TiZr alloy, with a surface area of 1.8 cm^2 and the Pt counter electrode.

AZ31 and TiZr alloy samples were characterized morphological, structurally, and electrochemically using the following equipment:

- *Electrochemical tests* were carried out to determine the corrosion resistance of both alloys and coatings using an AutoLab potentiostat.

- *Inductively coupled plasma mass spectrometry (ICP-MS)* was used for the determination of the concentration of ions in the SBF solution and *Fourier Transform Infrared Spectroscopy (FT-IR)* was used to determine the functional groups of sample coatings.

- *Scanning electron microscopy (SEM)* and *energy dispersive X-ray analysis (EDX)* were used to determine the surface morphology of the samples as well as the elemental composition of the coatings in this thesis.

- *The contact angle (CA)* was measured to determine the hydrophobicity of uncoated and coated alloy samples.

- *The surface roughness* of TiZr-PLA alloy samples was determined by using a roughness tester and an atomic force microscope (AFM).

- *Vickers microhardness (HV)* was performed to determine the hardness of uncoated and coated alloy samples using a Vickers hardness tester.

- *UV-VIS spectroscopy* was used for the encapsulation-release tests of drug from coated alloy sample using a UV spectrometer.

- *The adhesion strength* of the coatings was determined by pull-off tests using an adhesion tester.

- *BET (Brunauer-Emmett-Teller) analysis* was performed to determine the surface area and pore distribution of PLA coatings deposited on the AZ31 substrate.

CHAPTER V

SURFACE MODIFICATION OF THE AZ31 ALLOY WITH PLA

In this chapter, the surface of the AZ31 alloy has been modified using polylactic acid by two methods: deposition of nanofibers and films on the metal substrate. The synthesis, characterization, and comparison of the two alloy-deposited structures were studied to improve the properties of PLA nanofibers and films for potential applications. The presence of PLA was evidenced by structural and morphological analysis using FT-IR and SEM, as well as by adhesion strength and porosity analysis of coatings.

5.1. FT-IR analysis of PLA coatings

The presence of polylactic acid deposited on the surface of the AZ31 alloy was confirmed using Fourier Transform Infrared Spectroscopy (FT-IR) by the characteristic bands of polylactic acid as shown in Figure 5.1.

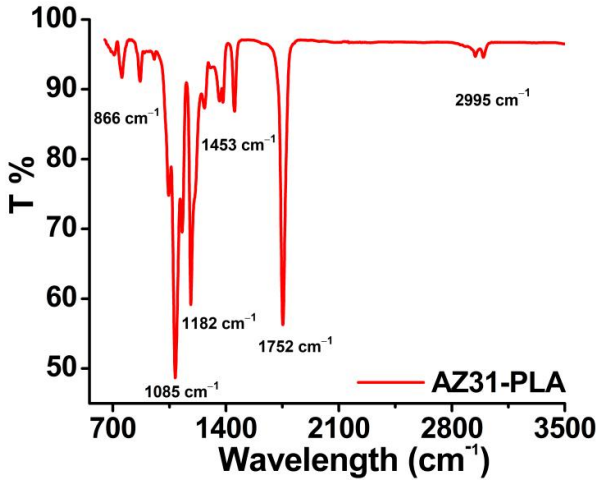

Figure 5.1. FT-IR spectrum of polylactic acid

5.2. Scanning electron microscopy (SEM)

SEM micrographs of the AZ31 alloy showed characteristic morphologies of polished metal alloy as well as of the two polymer structures deposited on the alloy surface by two methods: electrospinning and dip-coating.

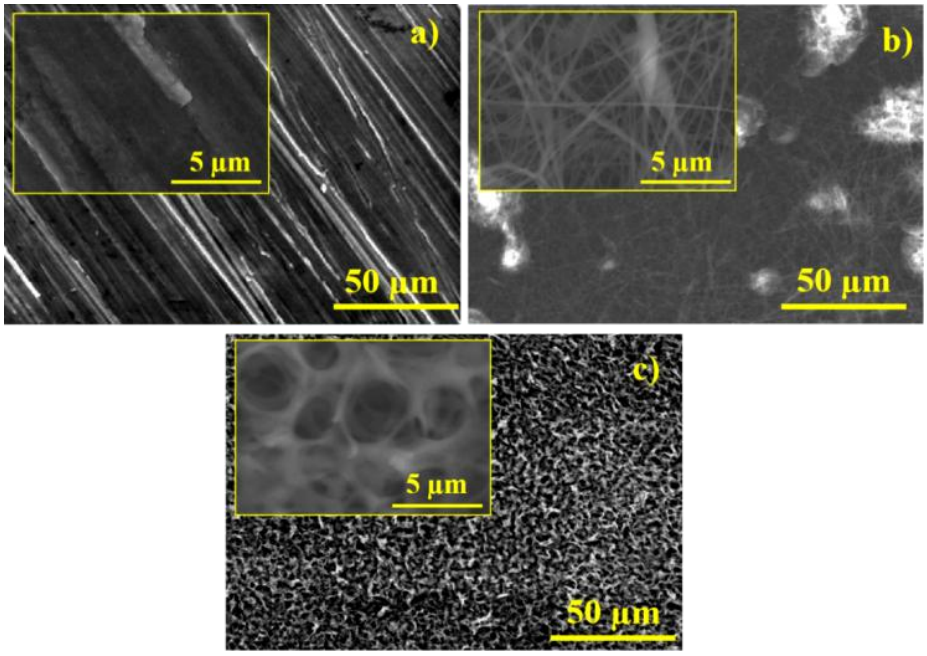

Figure 5.2. SEM micrographs of a) uncoated AZ31 alloy, b) AZ31-PLA nanofibers, and c) AZ31-PLA dip

5.4. Adhesion strength and BET analysis of coatings

The adhesion of PLA coatings on the AZ31 alloy surface was determined by pull-off tests, and the values are shown in Table 5.4.

As can be seen, the adhesion strength is higher for the AZ31-PLA dip sample compared to the AZ31-PLA nanofibers sample. Thus, the results showed that the dip-coating process leads to a coating with better adhesion.

Table 5.4. Adhesion strengths of AZ31 alloy samples

Sample	Adhesion strength [MPa]
AZ31-PLA nanofibers	1.66
AZ31-PLA dip	4.99

The BET method was used to determine the specific surface area and pore size of PLA coatings (Table 5.5.), and according to the results obtained, the dip-coating technique led to a mesoporous film with more voluminous pores than nanofibers coating, which may produce more promising results for drug encapsulation as well as better antibacterial activity.

Table 5.5. Data obtained from the BET analysis

Sample	Surface area [m^2/g]	Total pore volume [cm^3/g]	Pore diameter [nm]	Microporous surface [m^2/g]	Micropore volume [cm^3/g]
PLA dip	5.43	0.0066	3.30	13.71	0.0049
PLA nanofibers	12.09	0.0012	3.67	3.43	0.0012

CHAPTER VI

TESTING THE STABILITY OF AZ31 ALLOY IN SIMULATED BIOLIQUIDS

The bioactivity of AZ31 biodegradable alloy was evaluated by surface analysis following the evolution of apatite deposits grown on the surfaces of the alloy samples after immersion in SBF solution over time, as well as the evolution of hydrogen and pH variation in the uncoated and AZ31-PLA alloy samples.

6.1. Behavior of the uncoated AZ31 alloy in SBF

The behavior of AZ31 alloy in SBF solution was studied by immersing uncoated alloy samples in sterile flasks in a volume of SBF solution pH 7.4 and monitoring the bioactivity of the alloy at different time intervals (1, 3, 7, 21, and 28 days).

6.2. Determination of Ca and Mg ions by ICP-MS

ICP-MS analysis was performed to determine the concentration of Ca^{2+} and Mg^{2+} ions (Table 6.1.) present in the SBF solution after the uncoated AZ31 alloy was immersed in the solution for different time intervals.

ICP-MS analysis shows that over time, the amount of Mg^{2+} ions in the SBF solution decreases due to the possible formation of magnesium oxide (MgO) on the surface of the alloy, which increases in thickness following the number of days of immersion in SBF.

Table 6.1. The concentration of Ca^{2+} and Mg^{2+} ions over time

Time [days]	The concentration of elements analyzed - [mg/L]	
	Ca^{2+}	Mg^{2+}
1	7.7	87.5
3	6.87	67.11
7	6.57	48,52
21	3.94	18.61
28	4.11	14.74

6.3. FT-IR analysis of samples immersed in SBF at different times

AZ31 alloy immersed in SBF solution to determine its stability over time showed the evolution of phosphate (980 cm^{-1} and 1190 cm^{-1}) and hydroxyl (635 cm^{-1} and 3570-3690 cm^{-1}) groups.

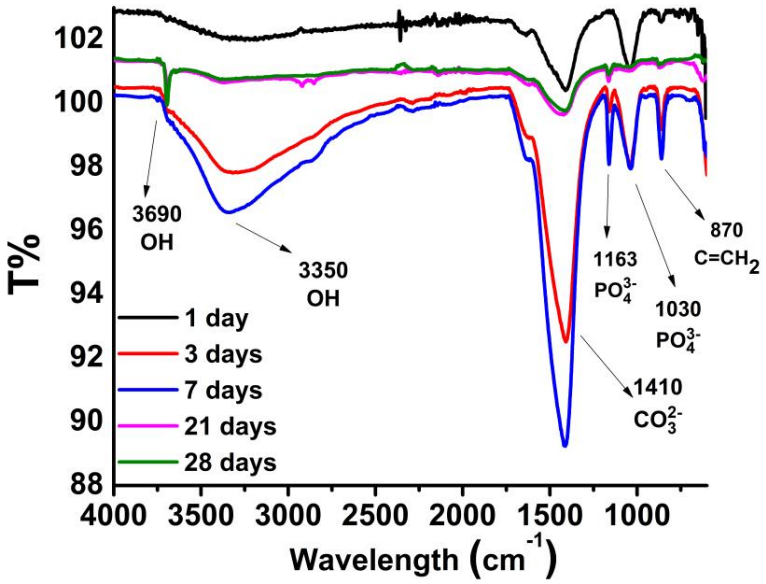

Figure 6.3. FT-IR spectra of AZ31 alloy samples investigated at different immersion times

6.4. Hydrogen evolution and pH variation of uncoated and AZ31-PLA alloy immersed in SBF

Hydrogen (H_2) release is one of the negative aspects of AZ31 alloy performance and was evaluated in SBF for both uncoated and PLA-coated AZ31 alloy at different time intervals (1h, 3h, 8h, 24h, 72h, 168h, 240h, 408h, and 504h).

The results of the H_2 volume evolution measurements for the uncoated AZ31 alloy sample and for the AZ31-PLA, as well as the pH variation of the SBF solution are, shown in Figure 6.5.

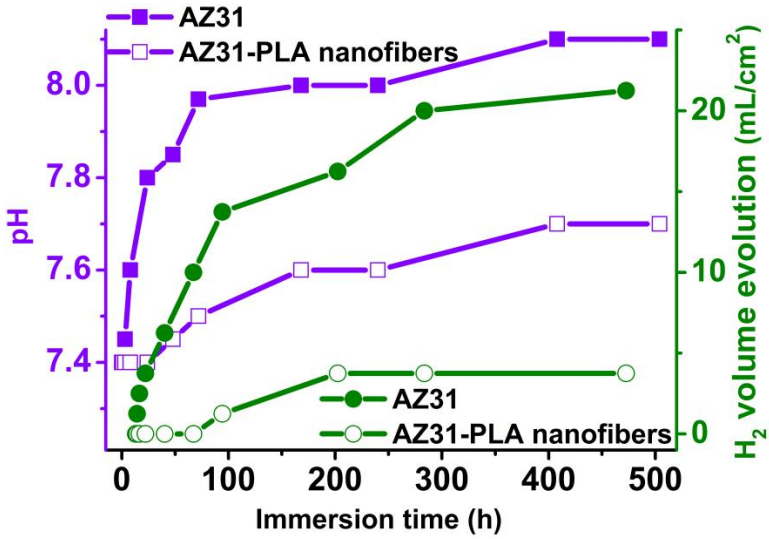

Figure 6.5. Time evolution of pH solution for uncoated AZ31 alloy and AZ31-PLA alloy samples in SBF solution for measurement of H2 evolution

Therefore, for the uncoated AZ31 alloy, after 504h of immersion, the total H_2 volume released was 21.25 mL/cm^2, compared to the AZ31-PLA alloy, which showed a total H^2 volume of 3.75 mL/cm^2.

6.5. Surface morphology of AZ31 alloy samples

The evolution of surface deposits on uncoated AZ31 alloy samples after immersion in SBF solution at different times was analyzed using SEM coupled with EDX.

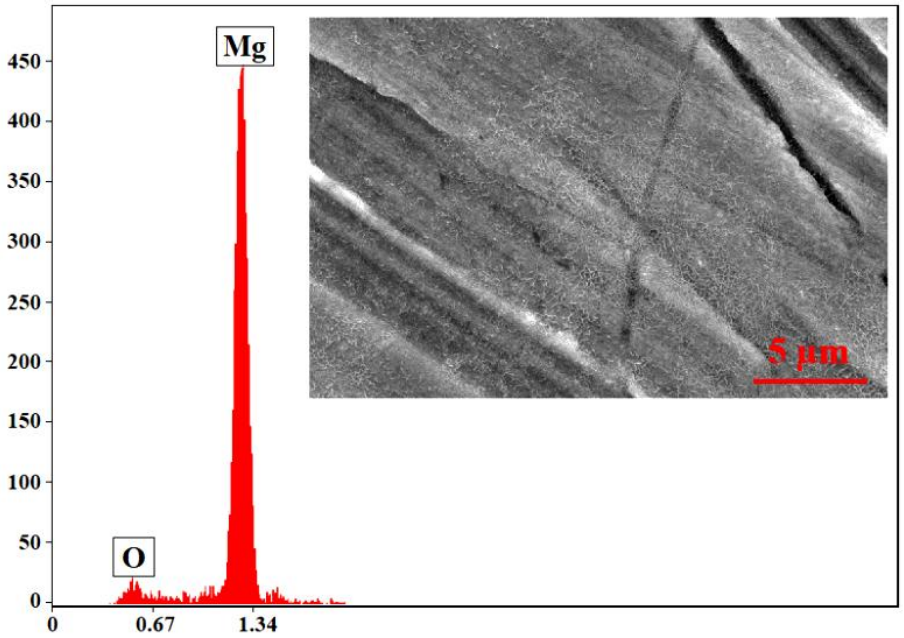

Figure 6.6. SEM morphology and EDX analysis for uncoated AZ31 alloy

On the surface of the AZ31 unimmersed alloy sample (Figure 6.6.), scratches can be seen that are the result of polishing. Small formations can also be seen, which are probably magnesium oxide (MgO) crystals.

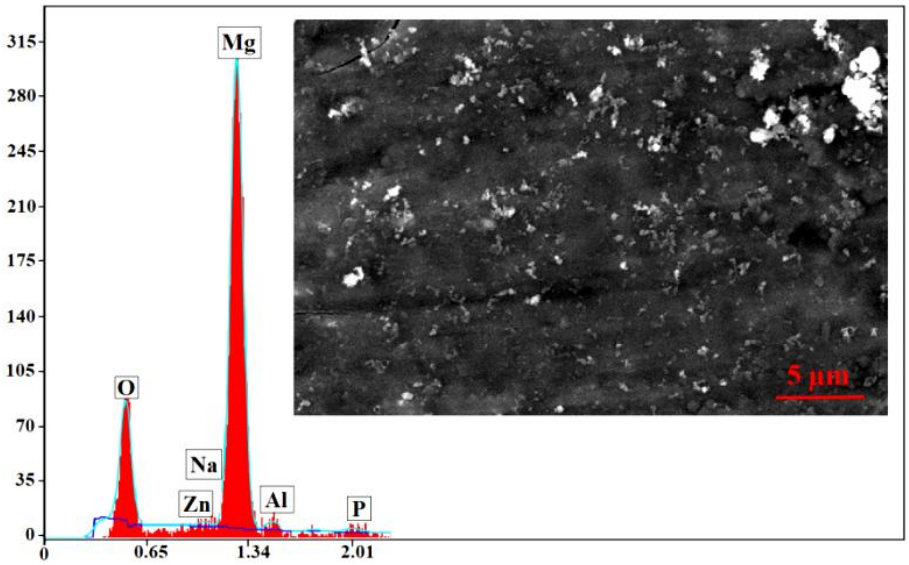

Figure 6.7. SEM morphology and EDX analysis of AZ31 alloy after 1 day of immersion in SBF

After one day of immersion in SBF (Figure 6.7.), crystals from the solution were deposited on the surface of the AZ31 alloy, with a base size of about 200 nm, but agglomerations can also be observed.

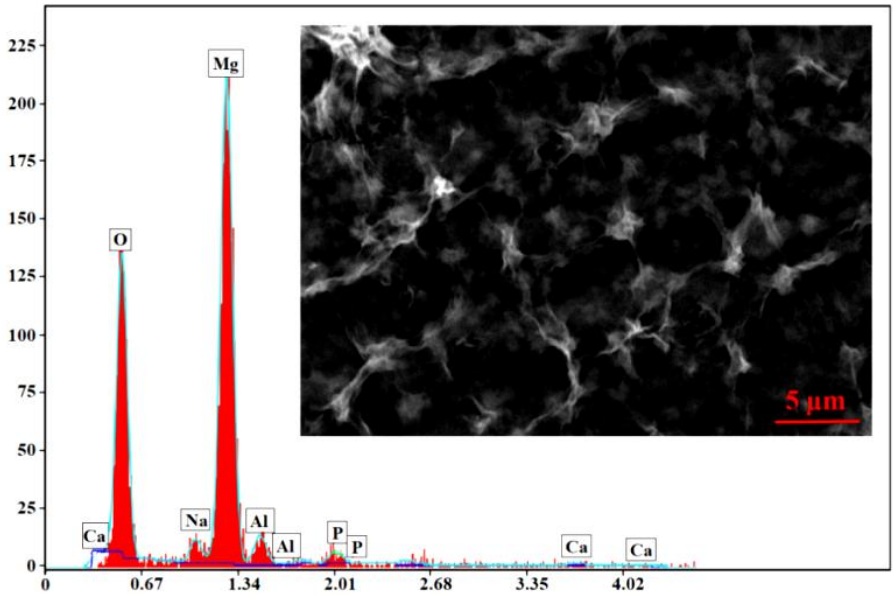

Figure 6.8. SEM morphology and EDX analysis of AZ31 alloy after 3 days of immersion in SBF

3 days after immersion (Figure 6.8.), the deposited crystals present a semi-self-organized network form with a central formation of about 1.5 µm diameter and ramifications of 2-4 µm length.

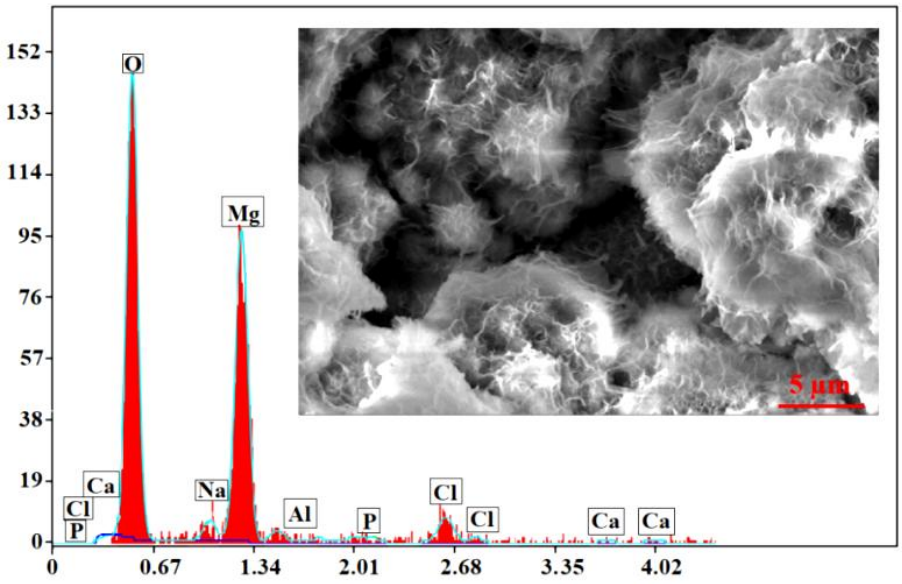

Figure 6.9. SEM morphology and EDX analysis of AZ31 alloy after 7 days of immersion in SBF

After 7 days of immersion (Figure 6.9.), crystals with the specific form of calcium phosphate are observed on the surface of the AZ31 alloy sample, with sizes between 2 and 10 µm.

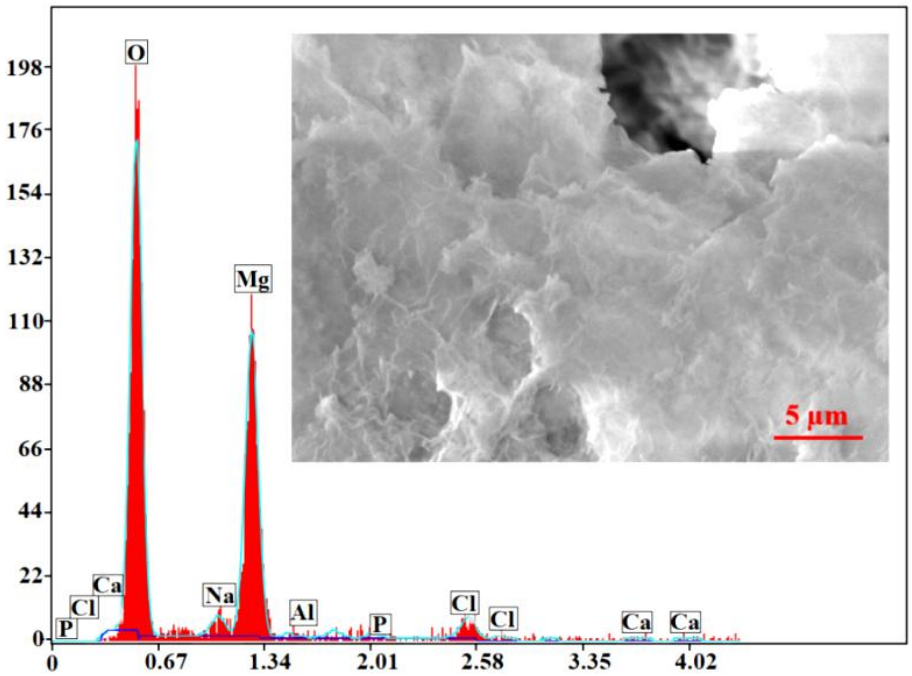

Figure 6.10. SEM morphology and EDX analysis of AZ31 alloy after 21 days of immersion in SBF

After 21 days of immersion (Figure 6.10.) on the AZ31 alloy sample, crystals of an irregular form and sizes of tens of µm can be observed.

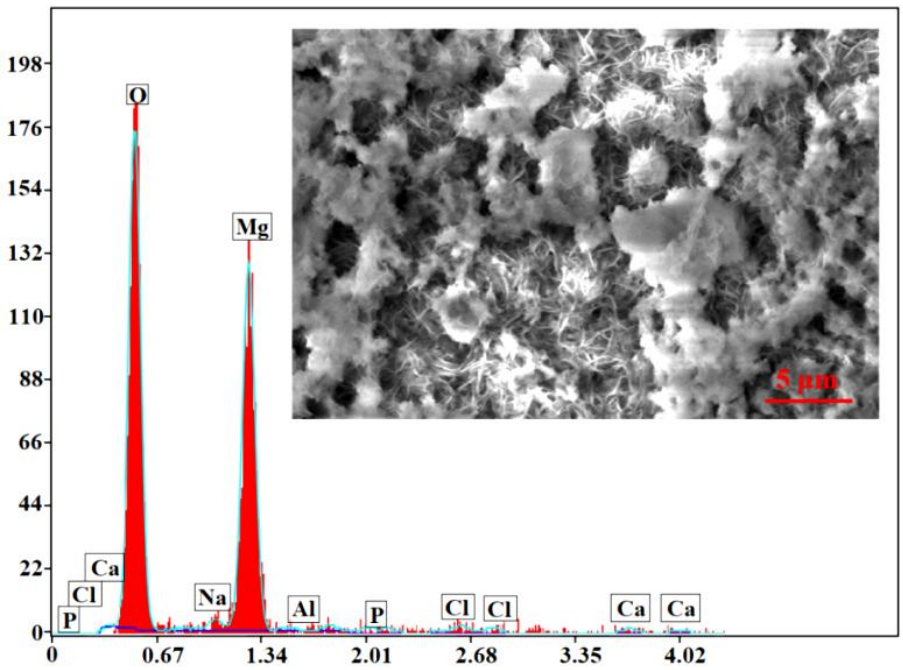

Figure 6.11. SEM morphology and EDX analysis of AZ31 alloy after 28 days of immersion in SBF

After 28 days of immersion (Figure 6.11.) two types of crystals can be observed: a cross-linked type, possibly calcium phosphate, and a cubic type, possibly sodium or calcium chloride. The dimensions of the cross-linked crystals are about 500 nm long and 50 nm wide, and the side length of a basic cubic crystal is about 500 nm.

CHAPTER VII

MODIFICATION OF THE TiZr SURFACE ALLOY

In the first part of this chapter, three different surface treatments of the non-biodegradable TiZr alloy (mechanical processing, acid pretreatment, and PLA nanofibre coatings) were investigated. The obtained results indicated that nanofibers coating improved the properties of the alloy compared to the uncoated alloy.

In the second part of this chapter, the electrochemical deposition of pyrrole from choline chloride-based ionic liquids concomitantly with the encapsulation of gentamicin sulphate on the TiZr alloy surface was realized for the first time in literature, which is original to this thesis. The obtained coatings were investigated morphologically and structurally, as well as in a kinetic study of drug release in phosphate buffered saline (PBS).

7.1. Coating TiZr alloy with PLA nanofibers

7.1.1. PLA coating morphology and sample roughness determination

The uncoated TiZr alloy samples and TiZr-PLA nanofibers samples were characterized using scanning electron microscopy. The surface of the TiZr sample exposed to acid pretreatment is completely coated with Ti and Zr oxides with lengths of 10-50 μm and widths of 2-5 μm. The TiZr-PLA sample indicates a complete coating of PLA nanofibers. The fibers are between about 250 and 450 nm in diameter and hundreds of micrometers in length.

The layer thickness of the PLA coating was investigated by AFM and is approximately 2.9 μm (Figure 7.1.d). Average roughness measurements (Figure 7.1.e) showed that the polished samples had the smoothest surface. Roughness increases after acid pretreatment due to the formation of oxide structures. The highest roughness value was obtained for the PLA nanofibers coated sample due to the multiple layers of polymer fiber bonding.

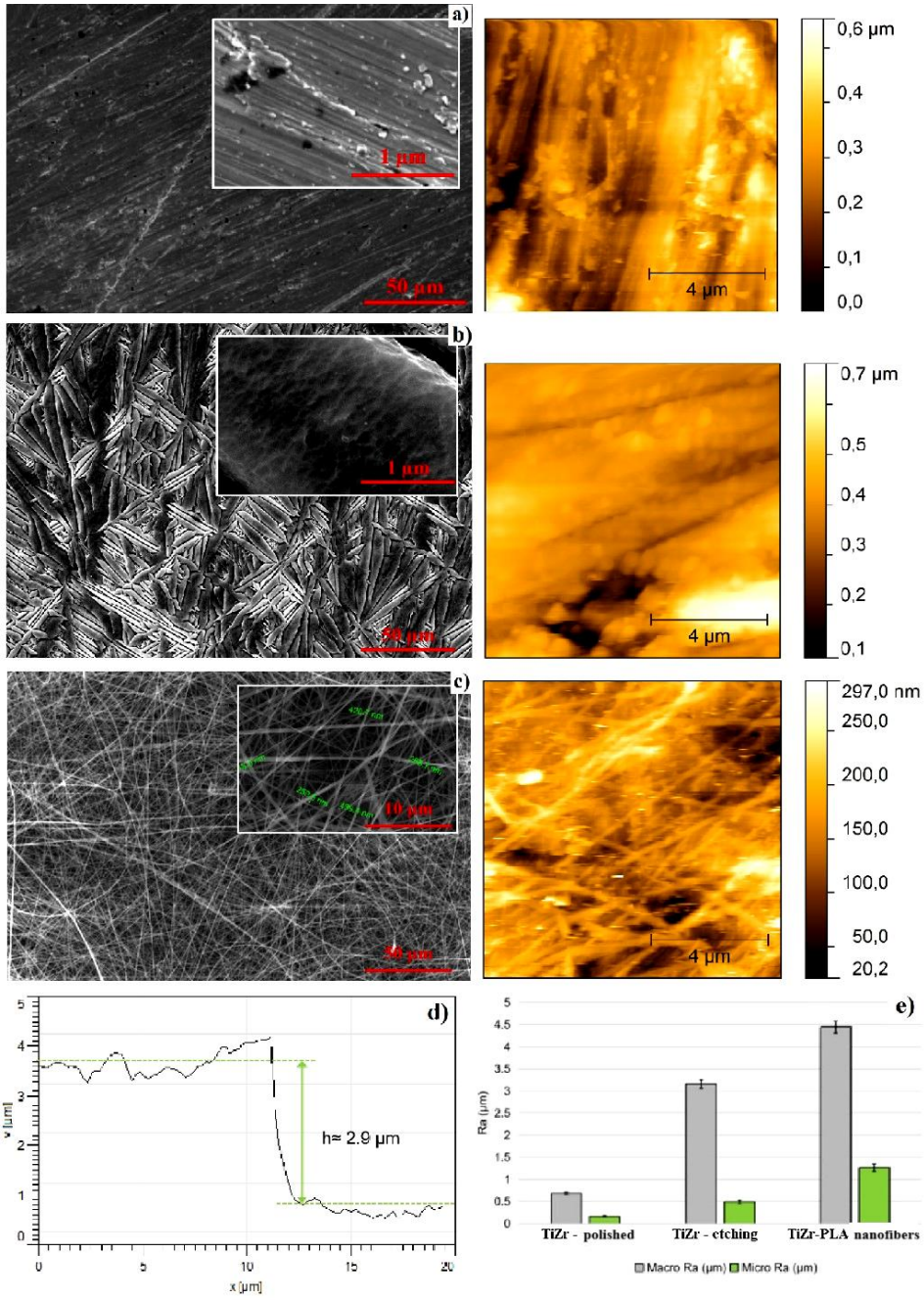

Figure 7.1. SEM morphology of a) polished TiZr, b) TiZr with acid pretreatment, c) TiZr-PLA nanofibers, d) cross-section of PLA coating, and e) average roughness values

7.1.2. Adhesion and hardness testing of TiZr alloy and PLA coating

Coating adhesion tests were performed using pull-off tests to measure the force needed to detach the coatings from the TiZr substrates. The adhesion forces measured during the experiments are shown in Table 7.1. The polished TiZr sample had the highest adhesion strength measured, followed by the acid-pretreated TiZr sample, and the weakest adhesion strength of all samples was measured for the PLA nanofibers coated sample.

Table 7.1. Adhesion strengths of TiZr samples

Sample	Adhesive strength [MPa]
TiZr polished	32.2 ± 0.6
TiZr acid pretreatment	21.4 ± 0.3
TiZr-PLA	4.3 ± 0.4

In the case of Vickers microhardness tests, the results are shown in Figure 7.2. The measured strengths determined during the experiment show that the hardest surface is TiZr polished alloy, followed by the oxidized sample, and the lowest value is the polymer layer.

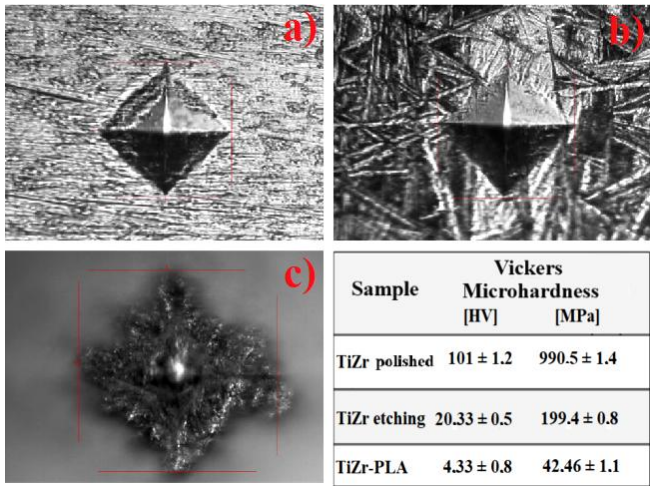

Figure 7.2. Sample morphology by Vickers microhardness: a) polished TiZr, b) TiZr with acid pretreatment (etching), c) TiZr-PLA nanofibers and calculated values

7.1.3. Contact angle analysis

Contact angle measurements indicated that the polished and acid-pretreated TiZr samples (Figure 7.3.a and b) have hydrophilic characteristics. Coating the TiZr surface with PLA nanofibers (Figure 7.3.c) increased the contact angle value, crossing the hydrophobicity limit.

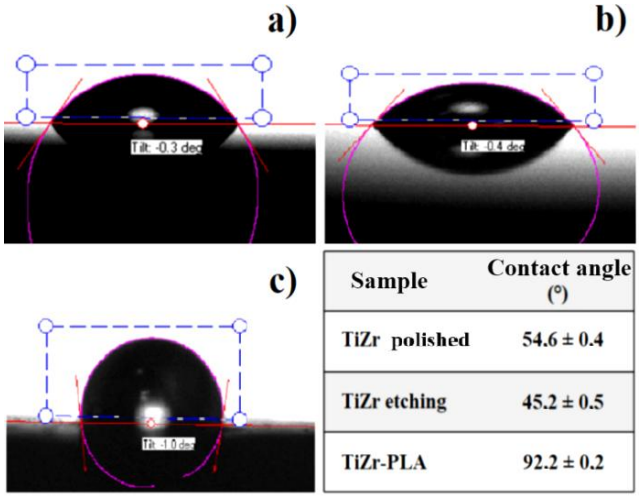

Figure 7.3. Contact angle measurements for a) polished TiZr, b) TiZr with acid pretreatment (etching), and c) TiZr-PLA nanofibers and contact angle values

7.2. Electropolymerization of polypyrrole and GS encapsulation on a TiZr alloy surface

7.2.1. Electropolymerization by cyclic voltammetry and chronoamperometry

The coating of TiZr alloy with PPy in NADES ionic liquid (choline chloride, lactic acid, and 0.5M pyrrole) used as an electrolyte was performed by cyclic voltammetry.

After electropolymerization of pyrrole on a TiZr substrate by cyclic voltammetry, chronoamperometry was applied to obtain PPy and PPy-GS films.

7.2.2. FT-IR analysis of polymer coatings

The evidence of PPy films as well as encapsulated GS films was analyzed using FT-IR measurements. The FT-IR spectra are shown in Figure 7.7. where the PPy and GS-specific peaks were identified. Also, characteristic peaks of the drug have been shown but shifted to a lower intensity due to possible chemical interactions generated during the coating process of PPy [138]. Thus, FT-IR analysis indicated the presence of GS in the PPy structure.

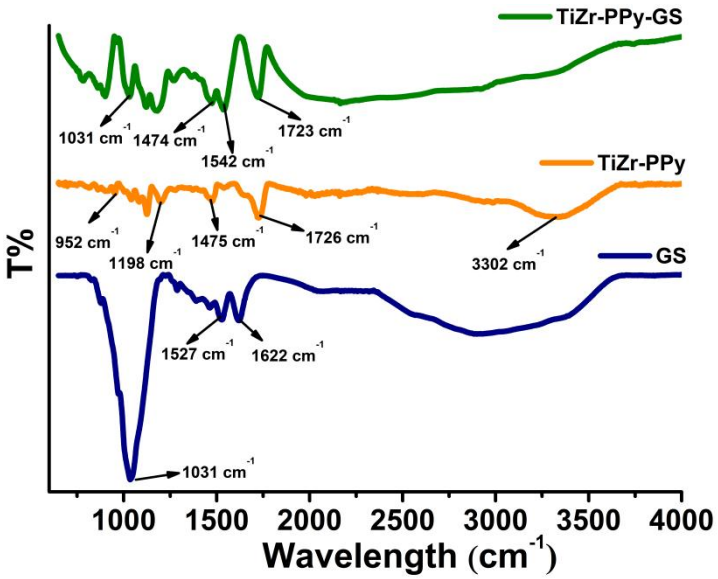

Figure 7.7. FT-IR spectra of TiZr alloy coated with PPy and TiZr-PPy encapsulated with GS

7.2.3. Morphological characterization of PPY and PPy-GS coatings

SEM analysis coupled with EDX was used to investigate the influence of electrodeposition parameters. The resulting SEM micrographs of the PPy and PPy-GS surfaces (Figure 7.8.) show a specific cauliflower structure of PPy and PPy-GS developed on the biomaterial surface under potentiostatic control in a NADES-based electrolyte.

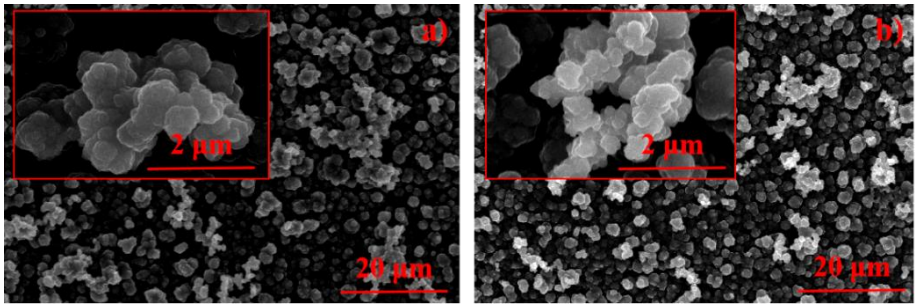

Figure 7.8. SEM morphologies for a) TiZr-PPy and b) TiZr-PPy-GS

Figure 7.9. represents the elemental analysis of PPy and PPy-GS films obtained with the EDX. In the case of GS-encapsulated polymer films, sulfur, and oxygen appear because the drug used contains sulfur ions in the chemical structure, which demonstrates the successful encapsulation of GS in the polymer coating.

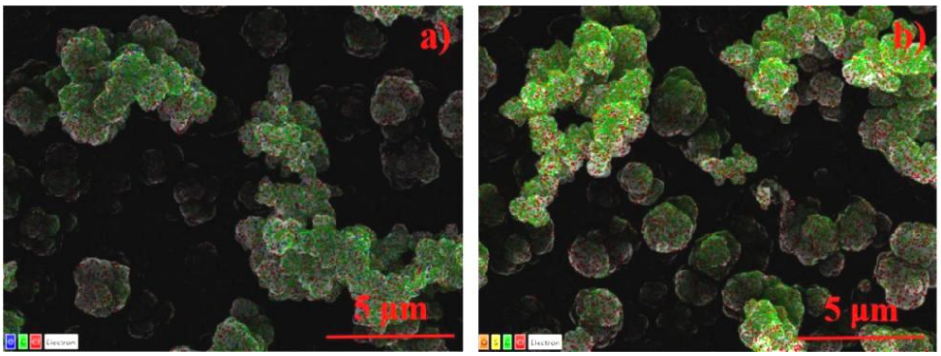

Figure 7.9. Surface elemental map obtained by EDX analysis for a) TiZr-PPy and b) TiZr-PPy-GS

7.2.5. Electrochemical tests

Electrochemical tests were performed using PBS pH 7.4 solution as an electrolyte for the uncoated TiZr alloy sample and for the polypyrrole coated and GS encapsulated sample.

The EIS method was applied to investigate chemical processes and changes that occurred in an electrochemical circuit. The results obtained from the samples analyzed are shown as Nyquist and Bode plots in Figure 7.11.

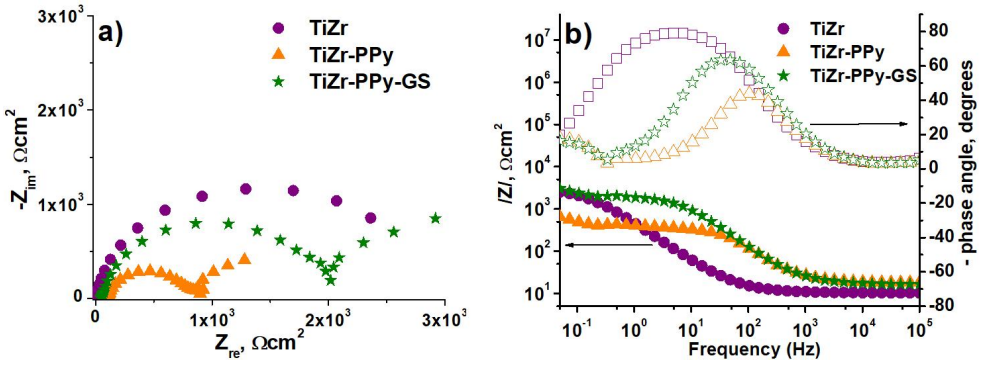

Figure 7.11. Diagrams a) Nyquist and b) Bode for uncoated, TiZr-PPy, and TiZr-PPy-GS, in PBS pH 7.4

Tafel potentiodynamic polarization tests are shown in Figure 7.12. showing a shift towards more electropositive values of the corrosion potential of coated TiZr compared to uncoated TiZr, as well as a decrease in corrosion current density, indicating that the polymer coating has a protective anti-corrosive effect.

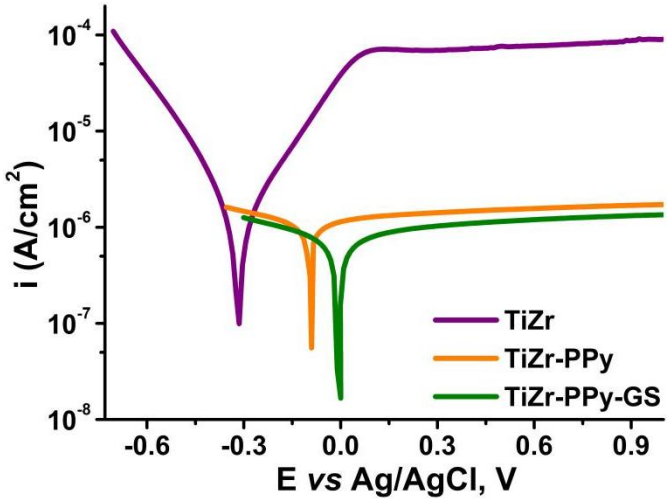

Figure 7.12. Tafel diagram for TiZr uncoated, TiZr-PPy and TiZr-PPy-GS, in PBS pH 7.4

Calculations of corrosion current density (icorr) and corrosion rate (CR) [139] for TiZr-PPy and TiZr-PPy-GS samples (Table 7.4.) showed a higher resistance to polarization compared to the uncoated alloy, indicating a decrease in the corrosion rate of each of the investigated biomaterials in PBS.

Table 7.4. The Tafel kinetic parameters for uncoated and coated TiZr alloy

Sample	*Tafel method*			
	E_{corr} [mV]	i_{corr} [µA·cm^{-2}]	K_g [g·m^{-2}h^{-1}]	CR [µm·an^{-1}]
TiZr	-0.295 ± 0.03	2.75 ± 0.02	0.0261 ± 0.001	8.44 ± 0.07
TiZr-PPy	-0.097 ± 0.01	0.603 ± 0.01	0.0057 ± 0.0003	1.85 ± 0.03
TiZr-PPy-GS	-0.006 ± 0.001	0.351 ± 0.01	0.0033 ± 0.0001	1.08 ± 0.01

7.2.6. Release of GS and antibacterial effect

TiZr alloy samples coated with polypyrrole and encapsulated with GS were tested for drug release in a 50 mL volume of pH 7.4 PBS solution. The analysis of the samples was performed at 203 nm wavelength and the cumulative release of GS was calculated.

The calibration curve showed a significant linear regression with a correlation coefficient of $R^2 = 0.9991$ from the equation obtained $y = 0.28445x + 0.12121$.

The GS release profile from polymer coatings electrodeposited on TiZr alloy using NADES electrolyte based on choline chloride and lactic acid containing 0.5M Py

and 0.05M GS is shown in Figure 7.14. The cumulative release of GS after 144h was about 90%, thus the PPy coatings may be able to release the drug over long periods.

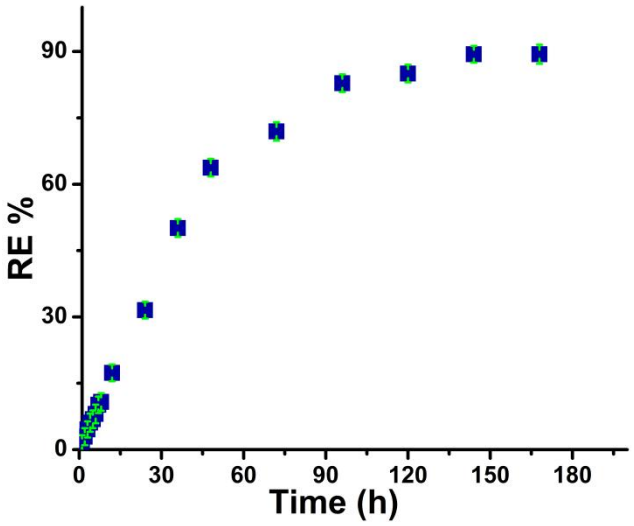

Figure 7.14. GS release profile of PPy coating

For the evaluation of the antibacterial effect, two types of gram-positive and gram-negative bacteria were used, *Staphylococcus aureus* and *Escherichia coli*.

The bacterial growth inhibition ratio (I%) is shown in Figure 7.15. for the three TiZr alloy samples. As can be seen, the coating significantly enhances the antibacterial activity of the samples.

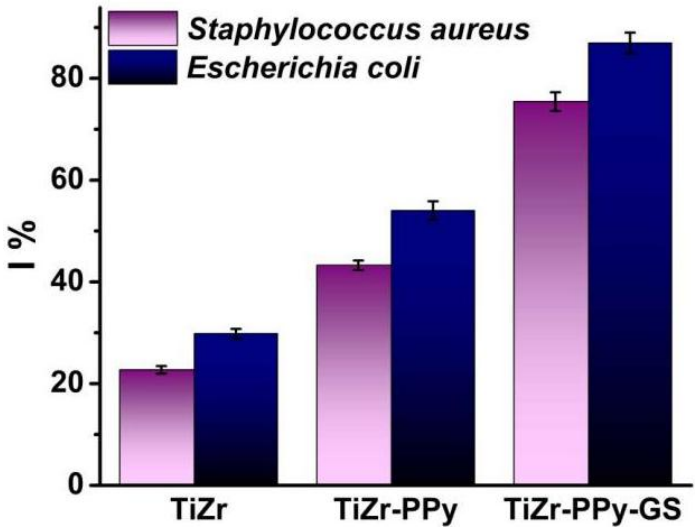

Figure 7.15. Bacterial inhibition for TiZr alloy samples

CHAPTER VIII

STUDY OF THE ELECTROCHEMICAL BEHAVIOR OF PLA ALLOYS

In this research, the PLA coatings deposited on AZ31 alloy substrate by two methods, nanofibers by electrospinning and films by dip-coating were investigated, and for TiZr alloy the coating consisted of just PLA nanofibers.

Uncoated and coated samples were investigated for corrosion resistance and electrochemical stability.

Electrochemical measurements were carried out with a potentiostat-galvanostat using an electrochemical cell with three electrodes: Ag/AgCl as the reference electrode (RE), Pt as the counter electrode (CE), and the working electrode (WE) consisting of the alloy samples.

The electrochemical methods used are open circuit potential (OCP), electrochemical impedance spectroscopy (EIS), and Tafel curves.

8.1. Electrochemical methods applied to uncoated and coated AZ31 biodegradable alloy by the two methods in SBF electrolyte

8.1.2. Electrochemical impedance spectroscopy (EIS) tests

Figure 8.2. represents Nyquist and Bode plots for uncoated AZ31 alloy and AZ31-PLA at different immersion times in SBF.

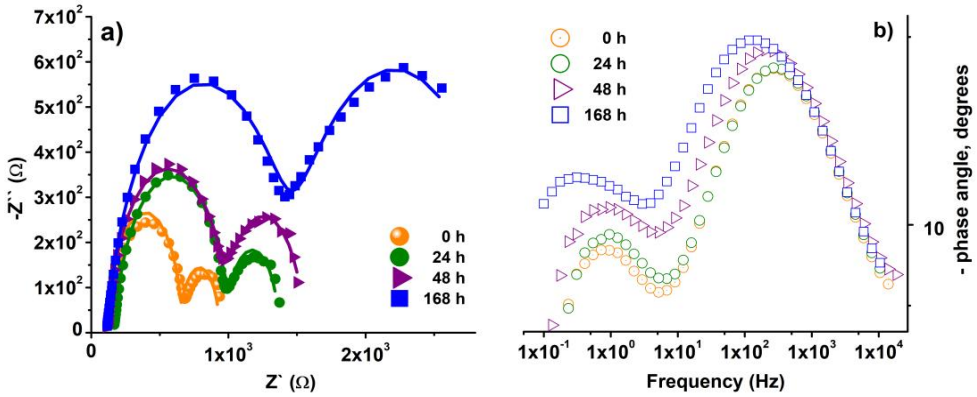

Figure 8.2. Diagrams a) Nyquist and b) Bode for uncoated AZ31 alloy immersed in SBF, over time

The Nyquist diagram of the AZ31 alloy presents, during the entire immersion time in the SBF solution, two defined loops with different diameters, indicating the same corrosion mechanism but with different corrosion rates [142].

The Bode phase diagram indicates that the phase angle shifts at low frequencies and increases slightly with immersion time. This is a consequence of the accumulation of corrosion products on the surface of the alloy, which leads to an increase in mass or an increase in thickness that could provide some protection [143].

From the EIS spectra, we can conclude that at 0h (Figure 8.3.a.), the AZ31 alloy was coated with thin oxides naturally produced in the atmosphere, and two capacitive loops were observed. A small capacitive loop at a high-frequency region could be attributed to the coating, while a large capacitive loop at a medium frequency region can be attributed to electrochemical processes occurring under the coating [144]. During immersion, corrosion products accumulated on the surface of the AZ31 alloy under the PLA nanofibers layer.

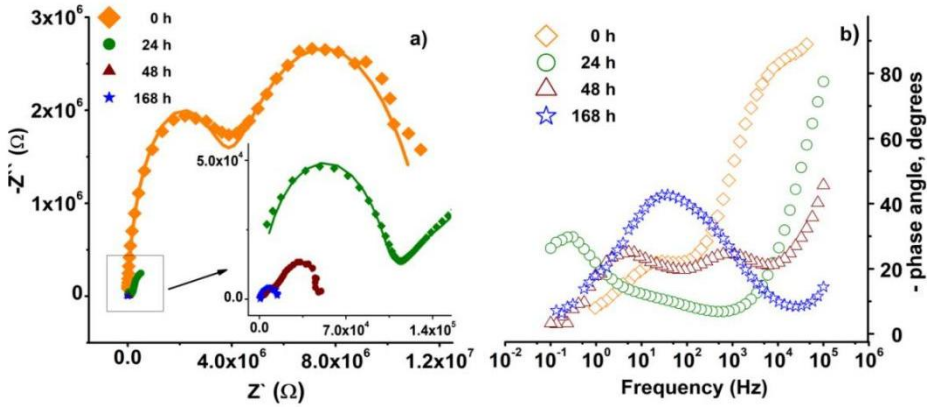

Figure 8.3. Diagrams a) Nyquist and b) Bode for AZ31-PLA nanofibers immersed in SBF, over time

Nyquist and Bode plots of the AZ31-PLA dip alloy are shown in Figure 8.4.a and Figure 8.4.b, respectively.

The Bode diagram shows the phase angle value of the AZ31-PLA dip immersed for 168h in SBF is more positive than the sample immersed for 0, 24, and 48h. This suggests a decrease in corrosion resistance has occurred.

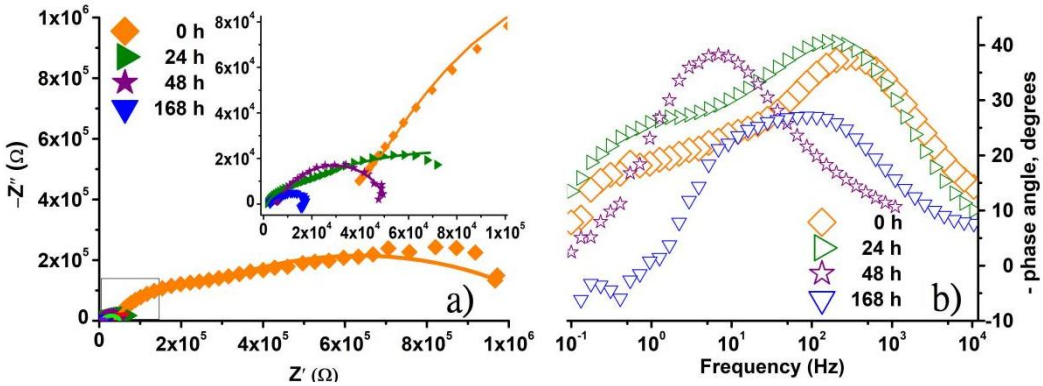

Figure 8.4. Diagrams a) Nyquist and b) Bode for AZ31-PLA dip immersed in SBF, over time

8.1.3. Tafel tests

Potentiodynamic curves were used to investigate the corrosion resistance of uncoated and coated AZ31 alloy.

According to Figure 8.5, the corrosion potentials at different immersion times in SBF solution of AZ31 alloy coated with PLA nanofibers and dipped are shifted towards

more positive values compared to uncoated AZ31 alloy. This suggests that both PLA coatings enhance the electrochemical stability of the AZ31 alloy.

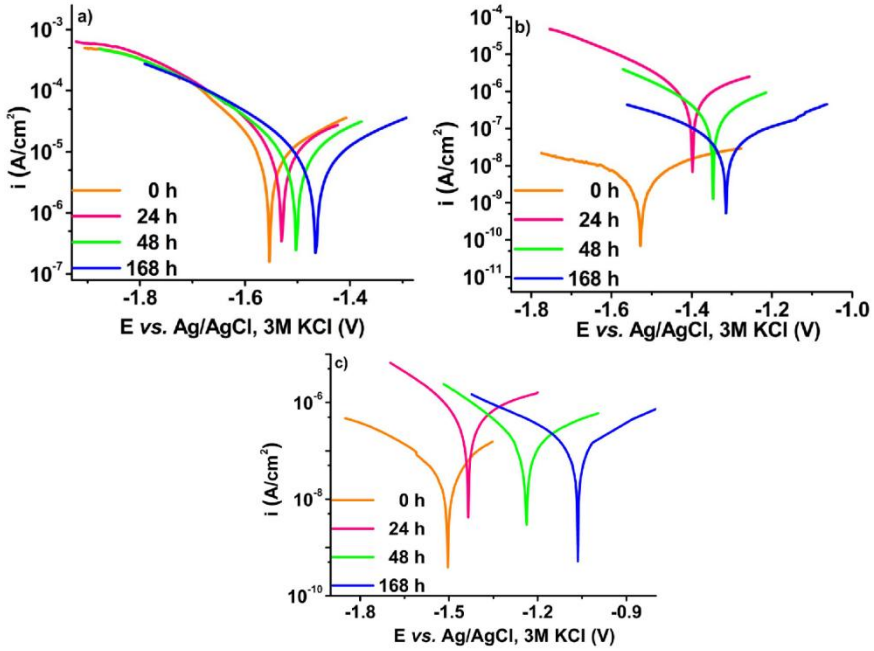

Figure 8.5. Tafel curves for a) uncoated AZ31 alloy, b) AZ31-PLA nanofibers, and c) AZ31-PLA dip, immersed in SBF solution, over time

8.2. Electrochemical methods applied to uncoated non-biodegradable TiZr alloy, coated with PLA nanofibers in different electrolytes

8.2.1. Electrochemical impedance spectroscopy (EIS) tests

Electrochemical impedance spectroscopy was used to characterize the oxide layers on TiZr samples and evaluate the performance of PLA coatings without accelerating electrochemical reactions at the sample/solution interface [148].

Figures 8.6. and 8.7. show the EIS spectra (Nyquist and Bode plots) for acid-pretreated TiZr samples in SBF and 0.9% NaCl, respectively.

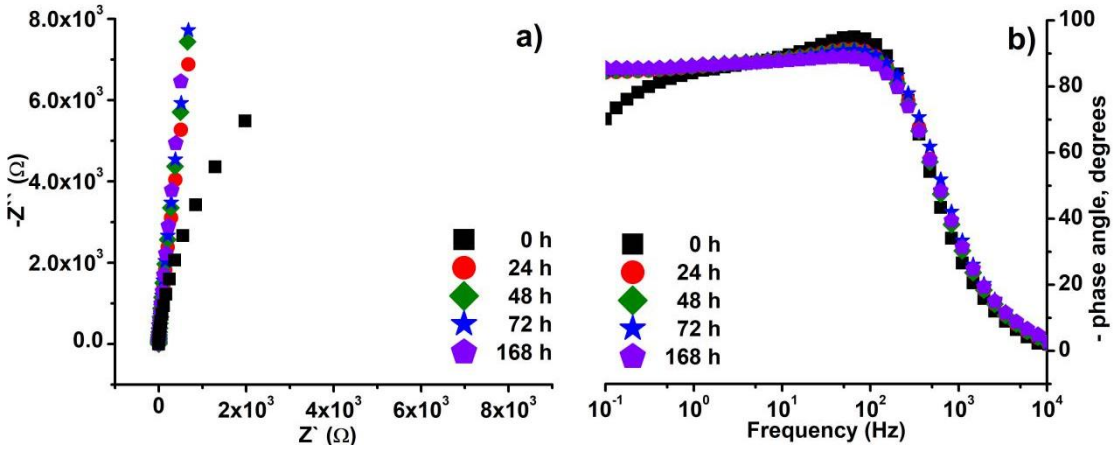

Figure 8.6. Diagrams a) Nyquist and b) Bode for TiZr with acid pretreatment in 0.9% NaCl

In 0.9% NaCl (Fig. 8.6.) the TiZr sample exposed to an acid pretreatment had a resistive response that increased with time. This can be attributed to the passive nature of the oxide formed, which has protective properties [149]. The Bode phase diagram shows TiZr samples have resistive resistance at high frequencies corresponding to charge transfer and capacitive resistance at low frequencies, suggesting that the diffusion process is dominant at lower frequencies.

Similar behavior was observed for samples immersed in SBF (Figure 8.7.).

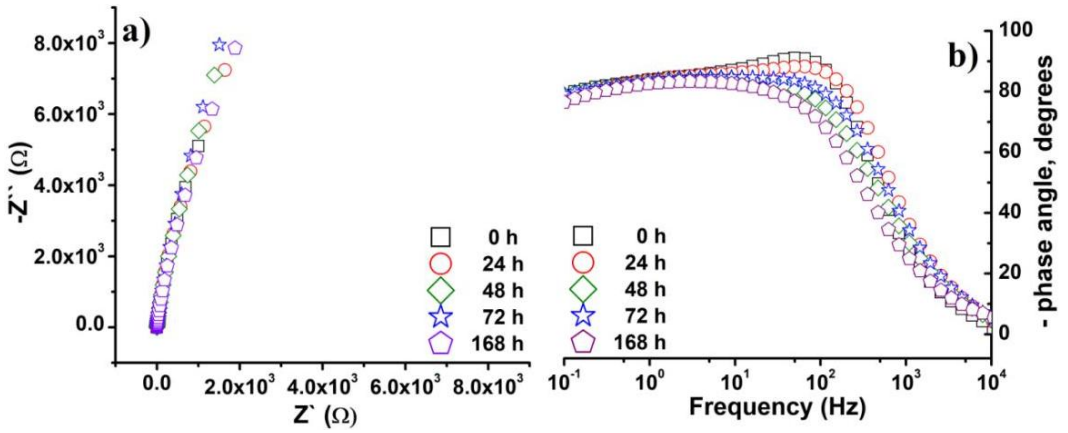

Figure 8.7. Diagrams a) Nyquist and b) Bode for TiZr with acid pretreatment in SBF

Figures 8.8. and 8.9. show the EIS spectra (Nyquist and Bode plots) for TiZr-PLA samples.

The TiZr-PLA sample immersed in 0.9% NaCl (Figure 8.8.) showed predominantly capacitive-diffusive behavior during the entire experiment.

In the Nyquist plot, the high impedance value at the initial immersion time was attributed to the air pockets between the PLA nanofibers. After the first day of immersion, the impedance value decreased and the samples showed more pronounced capacitive behavior.

The Bode phase diagram shows that TiZr-PLA has resistive behavior at low frequencies, diffusion occurring at medium frequencies, and pseudo-capacitive behavior at high frequencies which shifts to more resistive behavior with increasing immersion time.

The TiZr-PLA sample immersed in SBF (Figure 8.9.) had a higher resistive-diffusive behavior. At immersion time, the same high impedance attributed to the air pockets was observed in the Nyquist plot. After the first day, the impedance value decreases and the resistive behavior changes to diffusive.

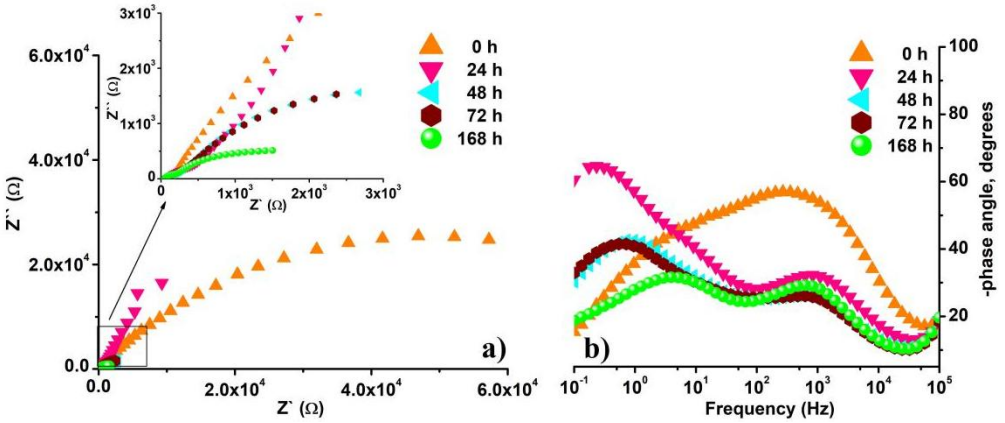

Figure 8.8. Diagrams a) Nyquist and b) Bode for TiZr-PLA in 0.9% NaCl

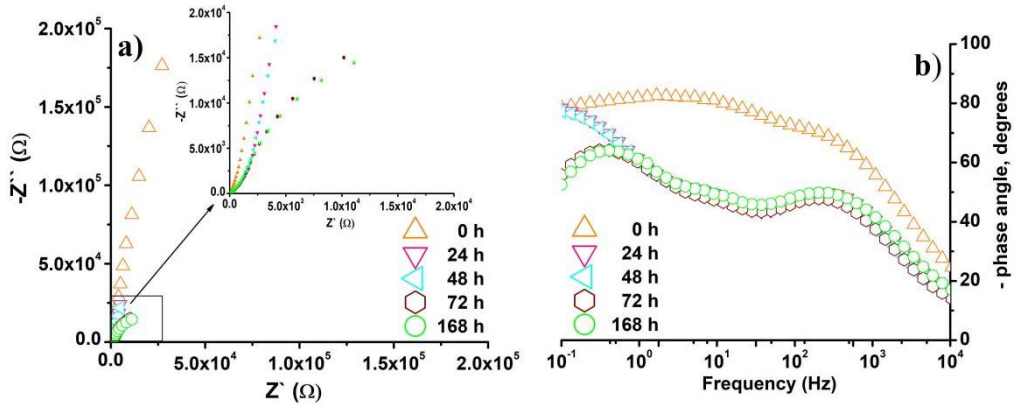

Figure 8.9. Diagrams a) Nyquist and b) Bode for TiZr-PLA in SBF

8.2.2. Tafel tests

Potentiodynamic polarization tests were used to evaluate the corrosion behavior of uncoated and PLA-coated TiZr samples over time, in 0.9% NaCl and SBF. Tafel plots are shown in Figures 8.10. and 8.11.

The TiZr sample with acid pretreatment (Figure 8.10.a) showed higher stability in 0.9% NaCl. The corrosion potential (E_{corr}) was stable at about -0.46 ± 0.025 V, the corrosion current (i_{corr}) decreased from 2.42 to 0.286 $\mu A \cdot cm^{-2}$ and the corrosion rate (V_{corr}) decreased from 7.43 to 0.879 µm/an.

In comparison, when the TiZr sample with acid pretreatment was immersed in SBF, the behavior was slightly different (Figure 8.10.b). The initial E_{corr} was more electronegative (-0.509 V) than measured in 0.9% NaCl, however, both i_{corr} (0.529 $\mu A \cdot cm^{-2}$) and V_{corr} (1.35 µm/an) had lower values.

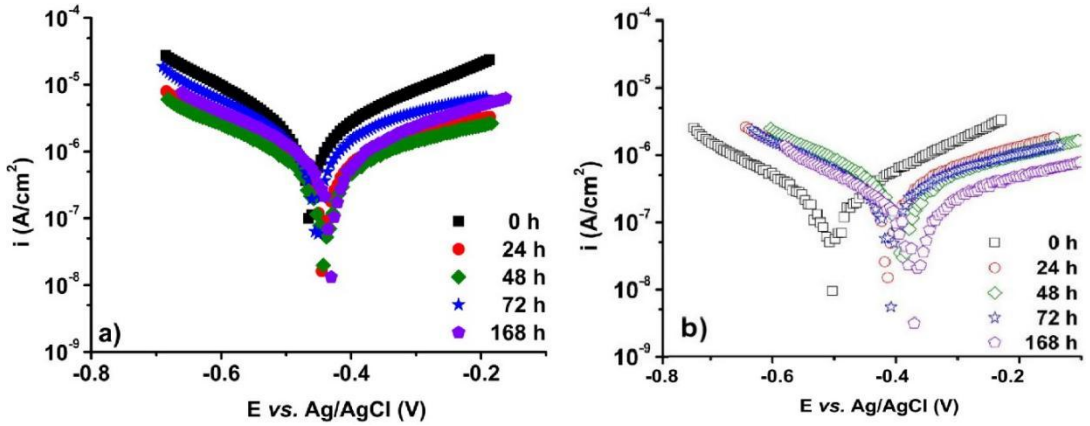

Figure 8.10. Tafel curves for a) TiZr with acid pretreatment in 0.9% NaCl and b) TiZr with acid pretreatment in SBF, over time

The TiZr-PLA nanofiber sample immersed in 0.9% NaCl (Figure 8.11.a) showed accelerated corrosion behavior over time. E_{corr} increased from -0.462 to -0.546 V, i_{corr} increased from 0.217 to 3.17 $\mu A \cdot cm^{-2}$, and V_{corr} increased from 2.22 to 32.46 μm/year.

Immersion in SBF of the TiZr-PLA nanofiber sample (Figure 8.11.b) showed a completely different result. Initially, the samples were practically inert. The samples showed corrosion characteristics after 24 hours of immersion.

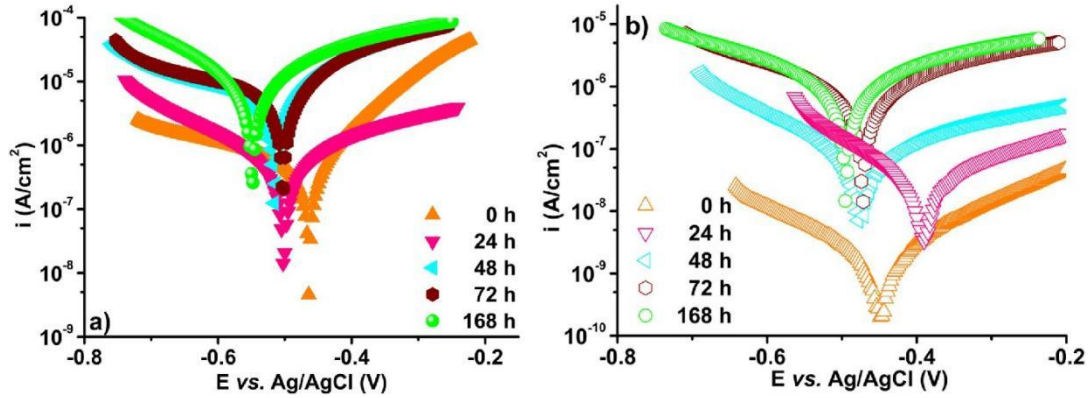

Figure 8.11. Tafel curves for a) TiZr-PLA in 0.9% NaCl and b) TiZr-PLA in SBF, over time

CHAPTER IX

STUDY OF ENCAPSULATION-RELEASE OF DRUG IN PLA COATINGS AND ANTIBACTERIAL ACTIVITY

The PLA coatings on biodegradable and non biodegradable metal substrates are used as drug delivery structures. The drug used was gentamicin sulfate (GS) dissolved in phosphate buffered saline (PBS). After encapsulation into PLA structures and determination of encapsulation efficiency, the presence of PLA and GS was determined by FT-IR analysis, and the morphology was observed by SEM.

In the release of the drug from polymeric structures, the kinetic model for each structure was determined by calculating the release efficiency. Also, due to the multiple infections that an implant could become infected with, antibacterial activity was determined for two of the most impacting bacteria, Escherichia coli and *Staphylococcus aureus*.

9.1. Encapsulation-release and antibacterial effect of PLA coatings on AZ31 alloy

9.1.1. GS encapsulation in PLA coatings obtained by electrospinning and dip-coating

The release of GS from PLA coatings deposited on AZ31 biodegradable alloy substrate by electrospinning and dip-coating was determined by immersing the samples in PBS solution and recording the UV spectra of the samples. The calibration curve showed a linear dependence of GS concentration given by Eq: Abs = 0.0105 + 5.922×10^{-4}C, with a correlation coefficient of $R^2 = 0.9990$.

The encapsulation efficiency for AZ31-PLA alloy samples was calculated and the results are shown in Figure 9.2. showing similar values for both types of samples, the dip-coated sample showing a slightly higher value. At 24h after immersion, 73% gentamicin was encapsulated in the dip-coated sample and 65% gentamicin was encapsulated in the nanofibers sample.

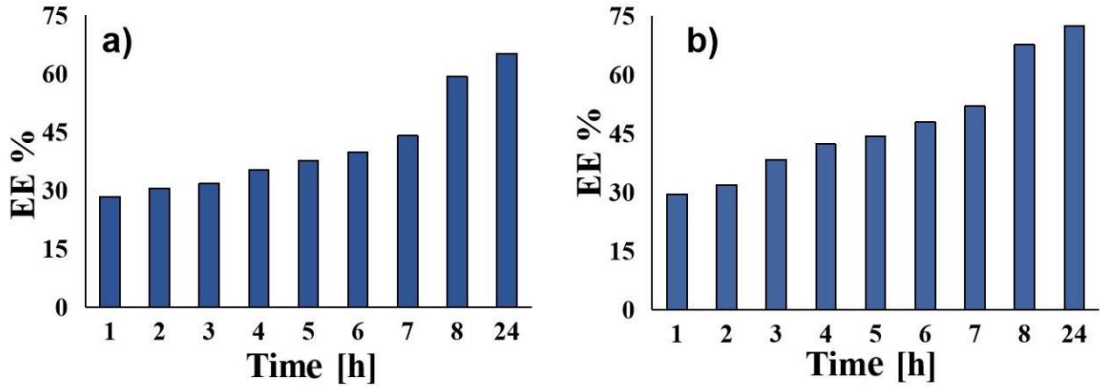

Figure 9.2. Encapsulation efficiency for a) AZ31-PLA-GS nanofibers and b) AZ31-PLA-GS dip

9.1.2. FT-IR analysis of drug presence

Encapsulation of GS in AZ31-PLA was confirmed by FT-IR analysis, and the spectra are shown in Figure 9.3. The characteristic bands of polylactic acid and gentamicin are observed. The existence of additional GS peaks in the AZ31-PLA spectra indicates that GS was encapsulated in the PLA coating.

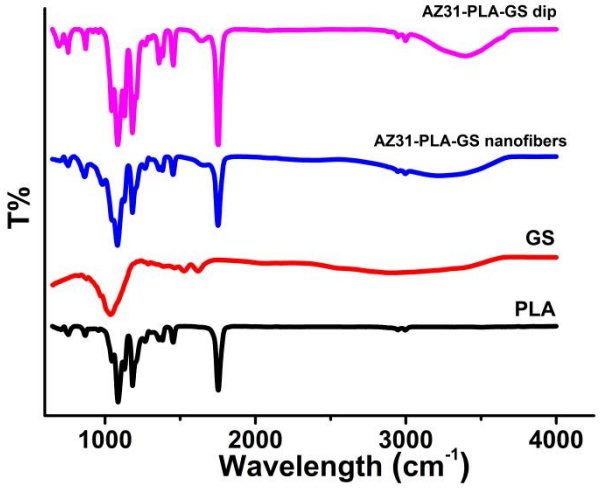

Figure 9.3. FT-IR spectrum for AZ31-PLA-GS

9.1.3. SEM analysis of drug coating morphology

SEM micrographs of the AZ31-PLA alloy samples encapsulated with GS are shown in Figure 9.4. GS particles are present in the nanofibers coating and also in the film coating as small bright dots of about 1 μm diameter.

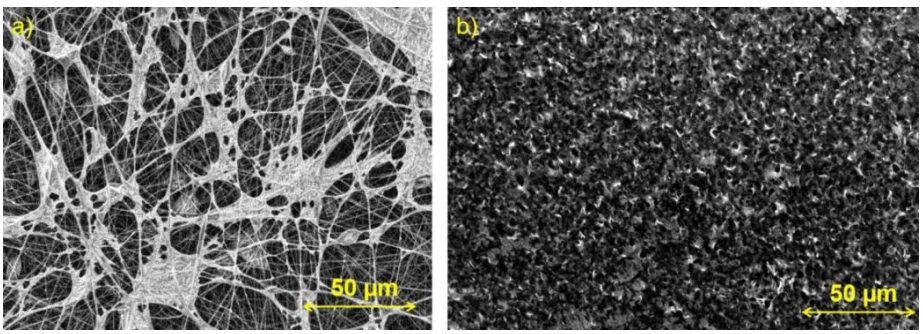

Figure 9.4. SEM micrographs for a) AZ31-PLA-GS nanofibers and b) AZ31-PLA-GS dip

9.1.4. Release of GS and fitting results

The release of GS encapsulated in AZ31-PLA nanofibers (Figure 9.5.) is slow during the entire release process. After 24h a small amount of GS (12.37%) was released, followed by a sustained release profile, meanwhile, for AZ31-PLA-GS dip samples, an increased amount of GS (49.53%) was released in 144h.

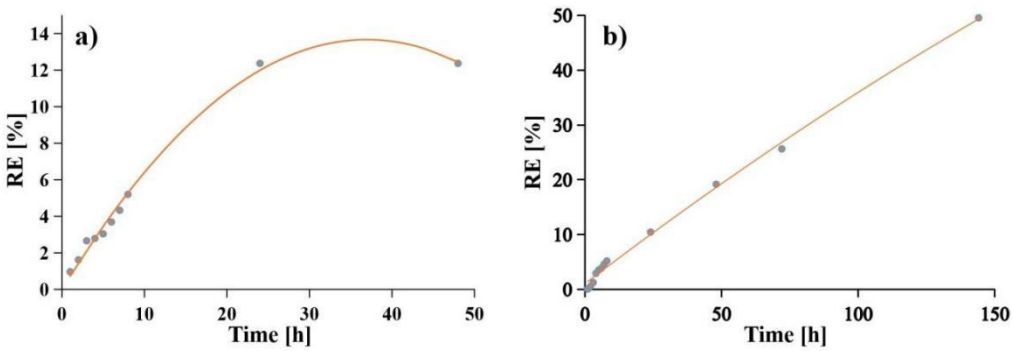

Figure 9.5. Release of GS from PLA coatings for a) AZ31-PLA-GS nanofibers and b) AZ31-PLA-GS dip

9.1.5. Antibacterial effect of AZ31 alloy samples

Antibacterial activity for AZ31 alloy samples (Figure 9.8.) was performed using *Escherichia coli* and *Staphylococcus aureus* bacteria. Optical density presented a higher antibacterial effect for *Staphylococcus aureus* compared to *E-coli* for both types of coatings. The experimental data showed that the dip-coated samples produced a higher antibacterial effect than the nanofibers coated samples. The addition of GS in both coatings increases the antibacterial effect.

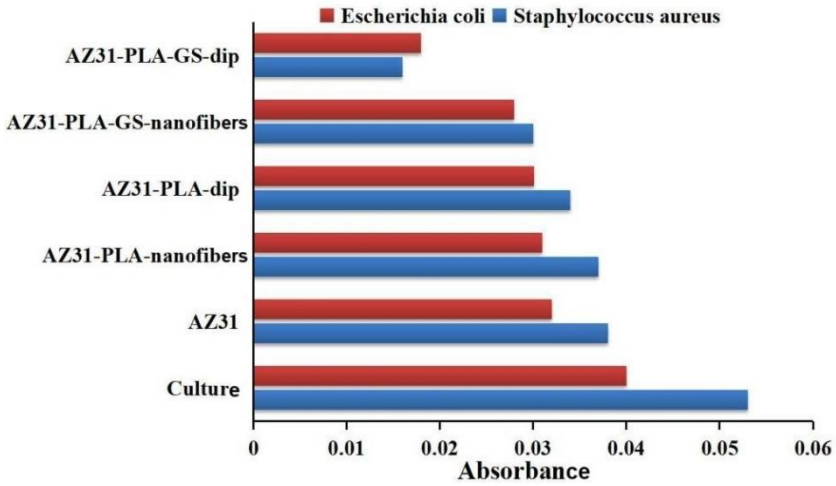

Figure 9.8. Antibacterial activity of AZ31-PLA-GS

9.2. Encapsulation-release and antibacterial effect of PLA nanofibers coating on TiZr alloy

9.2.1. GS encapsulation in PLA nanofibers

Drug encapsulation was optimized by immersing the samples in a 10 mL GS solution of concentration 2 g/L, and monitored spectral at wavelength λ = 194 nm, using a calibration curve in the concentration range 25-300 mg/L, with the equation Abs = 0.00321 + 9.0455×10^{-4}C and a correlation coefficient of R^2 = 0.9995. Encapsulation efficiency of 56.14% was obtained after 8h (Figure 9.10.).

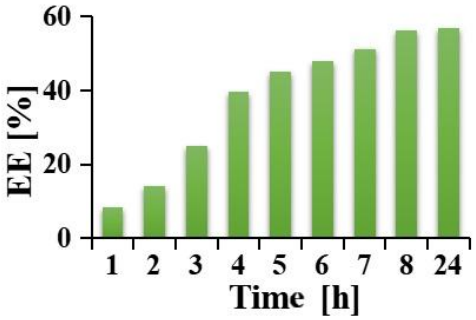

Figure 9.10. Graph of encapsulation efficiency of GS in PBS pH

9.2.2. FT-IR analysis of drug presence

Polylactic acid (PLA) nanofibers were characterized by Fourier transform infrared spectroscopy (FT-IR). The presence of gentamicin sulfate in PLA nanofibers was evidenced after 24h of encapsulation.

The FT-IR spectra of GS (Figure 9.11.) show peaks specific to the GS compound, and for GS-encapsulated PLA nanofibers, the FT-IR spectra show groups of both PLA and GS.

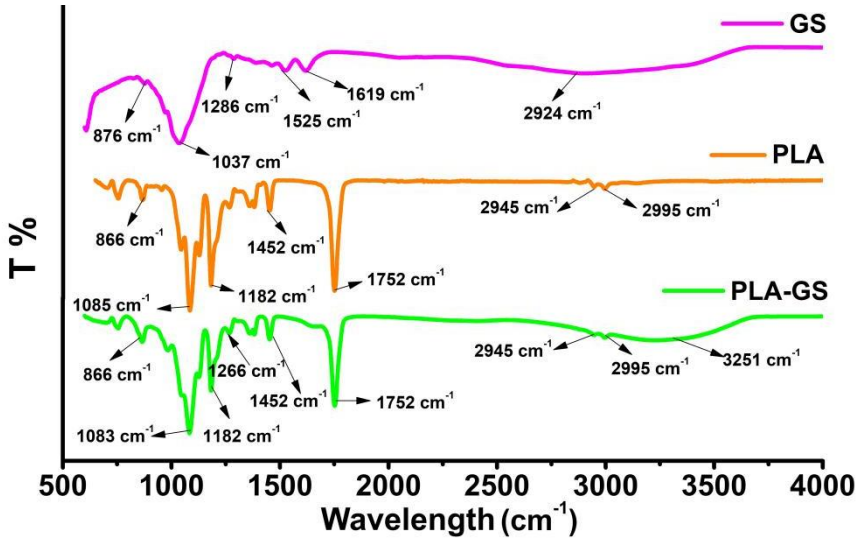

Figure 9.11. FT-IR spectra of TiZr-PLA-GS

9.2.4. Contact angle measurements

The PLA coating of the TiZr alloy and encapsulation of the drug in the PLA nanofibers modify the contact angle from hydrophilic values, similar to the uncoated TiZr alloy, to hydrophobic values, i.e. from 45° (uncoated TiZr, Figure 9.13.a) to 89.93° for TiZr alloy coated with PLA nanofibres (Figure 9.13.b) and 109.20 for TiZr-PLA-GS (Figure 9.13.c).

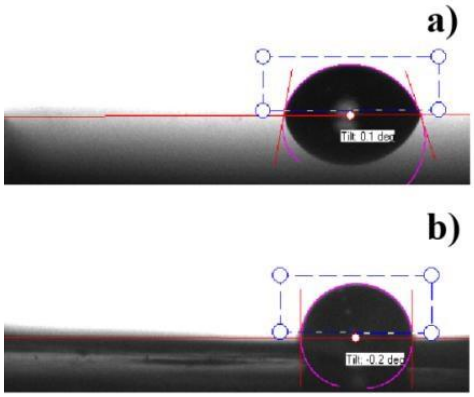

Sample	Contact angle (°)
TiZr etching	45
TiZr-PLA	89.93
TiZr-PLA-GS	109.20

Figure 9.13. Contact angle measurements for a) TiZr with acid pretreatment (etching), b) TiZr-PLA nanofibers, c) TiZr-PLA-GS and contact angle values

9.2.6. Release of GS and fitting results

The amount of gentamicin release was monitored using the spectral calibration curve at λ = 194 nm. A slow release of gentamicin into the receptor medium is observed, thus in the first hour 5.60% is released, and after 48h the release percentage is 40.33% (Figure 9.15.).

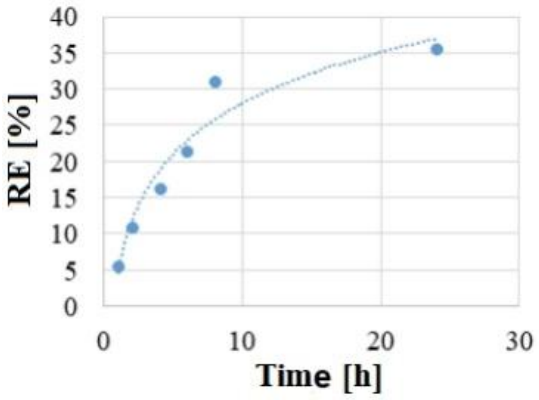

Figure 9.15. Release of GS from PLA nanofibers in PBS pH 5.8

9.2.7. Antibacterial effect of TiZr-PLA nanofibers alloy sample

Antibacterial activity evaluation was performed on an uncoated TiZr sample, coated with PLA nanofibers, and coated with PLA-GS encapsulated. The bacteria selected for our experiments were *Escherichia coli* and *Staphylococcus aureus* as gram-negative and gram-positive bacteria, respectively. The values obtained for the inhibition index are similar and the values are 30.29 for *Staphylococcus aureus* and 33.57 for *Escherichia coli*.

CONCLUSIONS

The coating of biodegradable and non-biodegradable alloys has been performed by various physicochemical and electrochemical methods leading to the development of structures used for encapsulation and drug release. The coating/physiological medium interface was studied by structural, morphological, and functional analyses.

Regarding the biodegradable alloy AZ31, the presence of PLA and drug in the polymer coating was evidenced using FT-IR spectroscopy. The PLA coating produced a hydrophobic surface.

The surface coating of AZ31 alloy with PLA by dip-coating shows a better adhesion compared to coating with PLA nanofibers.

Scanning electron microscopy (SEM) analysis showed hydroxyapatite formation and MgO growth on the surface of the biodegradable AZ31 alloy after immersion in SBF solution for 28 days. The characteristic structures of polymer coatings deposited on the surface of AZ31 alloy, nanofibers and film, respectively, were identified using SEM.

The two methods of fabrication (dip-coating and nanofibers) produced mesoporous PLA structures. The dip-coating showed more voluminous pores than the nanofiber coating, which permitted a higher drug encapsulation (73%) compared to the nanofiber coating (65%) as well as a higher GS release. Encapsulation of drug in mesoporous structures increased the antibacterial effect.

The coating of AZ31 alloy with PLA reduced the degradation rate of the alloy, which released a lower volume of H2 compared to uncoated AZ31 alloy, showing that the polymer coating improves the corrosion resistance of the alloy, which controls alloy degradation over time.

The PLA coatings improved the time stability of the alloys compared to the uncoated alloys in the SBF solution by shifting the corrosion potentials towards more electropositive values with increased immersion time and decreased corrosion rate, the coating acting as a barrier.

As an originality part, for the first time in the literature, polypyrrole coating of ionic liquids known as NADES was studied in TiZr alloy concomitant with drug encapsulation by electrochemical tests as cyclic voltammetry and chronoamperometry. Also, PLA nanofibers were deposited on the surface of TiZr alloy by electrospinning method.

The characteristic morphology of the polypyrrole coatings was identified using SEM and EDX was used to identify the elements present showing that the coating is uniform over the entire surface of the TiZr alloy.

Polypyrrole coating and the presence of the drug in the polymer structures were identified using FT-IR analysis.

The coating of PLA nanofibers on the TiZr alloy surface changes the surface physicochemical properties of the alloy (wettability, roughness, adhesion strength) and the electrochemical stability in the two electrolytes tested.

Encapsulation of the drug in both types of coatings deposited on TiZr substrate contributed significantly to increased antibacterial activity against gram-positive and gram-negative bacteria.

In conclusion, the polymer coatings studied improved the properties of the biodegradable and non-biodegradable alloys and efficient encapsulation of the drug leading to a better candidate for medical applications.

SELECTIV BIBLIOGRAPHY

[1].D.F. Williams, *Definitions in biomaterials: proceedings of a consensus conference of the European Society for Biomaterials*, Elsevier, Amsterdam, New York, **1987**

[2].D.F. Williams, *On the mechanisms of biocompatibility*, Biomaterials, Volume 29, pages 2941-2953, **2008**

[6].C. Jingtao, *Research of Magnesium-based Alloys for Medical Application*, 2nd International Conference on Education Technology and Information System, **2014**

[8].Y. Su, C. Luoa, Z. Zhanga, H. Hermawanc, D. Zhue, J. Huanga, Y. Lianga, G. Lib, L. Rena, *Bioinspired surface functionalization of metallic biomaterials*, Journal of the Mechanical Behavior of Biomedical Materials, Volume 77, pages 90−105, **2018**

[9].A. Kurup, P. Dhatrak, N. Khasnis, Surface modification techniques of titanium and titanium alloys for biomedical dental applications: A review, Materials Today: Proceedings, **2020**, https://doi.org/10.1016/j.matpr.2020.06.163

[20].A. X.Y. Guo, L. Cheng, S. Zhan, S. Zhang, W. Xiong, Z. Wang, G. Wang, S.C. Cao, *Biomedical applications of the powder-based 3D printed titanium alloys: A review*, Journal of Materials Science & Technology, Volume 125, pages 252−264, **2022**

[21].M. Prodana, C.-E. Nistor, A. B. Stoian, D. Ionita, C. Burnei, *Dual Nanofibrous Bioactive Coatings on TiZr Implants*, Coatings, Volume 10, page 526, **2020**, doi:10.3390/coatings10060526

[22].M. Sarraf, E.R. Ghomi, S. Alipour, S. Ramakrishna, N.L. Sukiman, *A state-of-the-art review of the fabrication and characteristics of titanium and its alloys for biomedical applications*, Bio-Design and Manufacturing, Volume 5, pages 371−395, **2022**

[26].A. Pantazi, M. Vardaki, G. Mihai, D. Ionita, A.B. Stoian, M. Enachescu, I. Demetrescu, *Understanding surface and interface properties of modified Ti50Zr with Nanotubes*, Applied Surface Science, Volume 506, 144661, **2020**

[28].D. Ionita, C. Pirvu, A.B. Stoian, I. Demetrescu, *The Trends of TiZr Alloy Research as a Viable Alternative for Ti and Ti16 Zr Roxolid Dental Implants*, Coatings, Volume 10, 422, **2020**

[29].G. Chandra, A. Pandey, *Preparation Strategies for Mg-Alloys for Biodegradable Orthopaedic Implants and Other Biomedical Applications: A Review*, IRBM, 43, pages 229−249, **2022**

[31].G. Chandra, A. Pandey, *Preparation Strategies for Mg-Alloys for Biodegradable Orthopaedic Implants and Other Biomedical Applications: A Review*, IRBM, Volume 43, pages 229−249, **2022**

[32].M. Echeverry-Rendon, J. P. Allain, S. M. Robledo, F. Echeverria, M. C. Harmsen, *Coatings for biodegradable magnesium-based supports for therapy of vascular disease: A general view*, Materials Science & Engineering C, Volume 102, pages 150−163, **2019**

[33].S. Höhn, S. Virtanen, A. R. Boccaccini, *Protein adsorption on magnesium and its alloys: A review*, Applied Surface Science, Volume 464, pages 212−219, **2019**

[34].M. Liyan, N. Jia, *In vitro biocorrosion and biocompatibility of AZ31 modified with magnesium phosphate coating by chemical deposition*, Surfaces and Interfaces, Volume 14, pages 208−214, **2019**

[42].A. Kurup, P. Dhatrak, N. Khasnis, S*urface modification techniques of titanium and titanium alloys for biomedical dental applications: A revie*w, Materials Today: Proceedings, **2020**, https://doi.org/10.1016/j.matpr.2020.06.163

[43].P. R. Chowdhury, S. Vahabzadeh, *Deposition of magnesium on surface- modifed titanium for biomedical applications*, Journal of Materials Research, Volume 37, pages 2635−2644, **2022**, DOI:10.1557/s43578-022-00611-4

[49].R. Hedayati, S. M. Ahmadi, K. Lietaert, N. Tumer, Y. Li, S. A. Yavari, A. A. Zadpoor, *Fatigue and quasi-static mechanical behavior of bio-degradable porous biomaterials based on magnesium alloys*, Journal of Biomedical Materials Research Part A, Volume 106, Issue 7, pages 1798–1811, **2018**

[50].H. Moldovan, E. Plopeanu, G. Dan, M. Vasilescu, M. Dobrescu, C. Milea, K. Earar, D. Gheorghita, *Contributions on biodegradability of Mg-Ca alloys for orthopedic implants*, UPB Scientific Bulletin, Series B: Chemistry and Materials Science, Volume 80, Issue 4, pages 229–246, **2018**

[64].R. Ion, A.B. Stoian, C. Dumitriu, S. Grigorescu, A. Mazare, A. Cimpean, I. Demetrescu, P. Schmuki, N*anochannels formed on TiZr alloy improve biological response*, Acta Biomater., Volume 24, pages 370–377, **2015**

[66].J. Alipal, N.A.S. Mohd Pu'ad, N.H.M. Nayan, N. Sahari, H.Z. Abdullah, M.I. Idris, T.C. Lee, *An updated review on surface functionalisation of titanium and its alloys for implants applications*, Materials Today: Proceedings, Volume 42, pages 270–282, **2021**, https://doi.org/10.1016/j.matpr.2021.01.499

[67].D. Aggarwal0, V. Kumar, S. Sharma, *Drug-loaded biomaterials for orthopedic applications: A review*, J Control Release, Volume 344, pages 113–133, **2022**

[68].M. Skwarczynski, S. Bashiri, Y. Yuan, ZM. Ziora, O. Nabil O, K. Masuda, M. Khongkow, N. Rimsueb, H. Cabral, U. Ruktanonchai, MAT. Blaskovich, I. Toth, A*ntimicrobial Activity Enhancers: Towards Smart Delivery of Antimicrobial Agents*, Antibiotics (Basel), Volume 11, Issue 3, pages 1–28, **2022**

[70].J.D. Luo, C. Miller, T. Jirjis, M. Nasir, D. Sharma, *The effect of non-steroidal anti-inflammatory drugs on the osteogenic activity in osseointegration: a systematic review,* Int J Implant Dent., Volume 4, Issue 1, page 30, **2018**, doi: 10.1186/s40729-018-0141-7

[72].A. B. Stoian, I. Demetrescu, D. Ionita, *Nanotubes and nano pores with chitosan construct on TiZr serving as drug*, Reservoir, Colloids and Surfaces B: Biointerfaces, Volume 185, 110535, **2020**

[73].F. Tao, S. Ma, H. Tao, L. Jin, Y. Luo, J. Zheng, W. Xiang, H. Deng, *Chitosan-based drug delivery stems: From synthesis strategy to osteomyelitis treatment – A review,* Carbohydr Polym., Volume 251, pages 1–15, 117063, **2021**

[74].AO. Fadaka, NRS. Sibuyi, AM. Madiehe, M. Meyer, *Nanotechnology-based delivery systems for antimicrobial peptides*, Pharmaceutics, Volume 13, Issue 11, pages 1−25, 1795, **2021**

[75].I. Demetrescu, C. Dumitriu, G. Totea, C.I. Nica, A. Dinischiotu, D. Ionita, *Zwitterionic cysteine drug coating influence in functionalization of implantable Ti50Zr alloy for antibacterial, biocompatibility and stability properties*, Pharmaceutics, Volume 10, Issue 4, 220, pages 1–18, **2018**

[76].JLP. Gemeinder, NR. de Barros, G. Sant'Ana Pegorin, J. de Lacorte Singulani, FA. Borges, MC. Gabriel Del Arco, MJ. Soares Mendes Giannini, AM. Fusco Almeida, SL. de Souza Salvador, RD. Herculano, *Gentamicin encapsulated within a biopolymer for the treatment of Staphylococcus aureus and Escherichia coli infected skin ulcers,* J Biomater Sci Polym Ed., Volume 32, Issue 1, pages 93–111, **2021**

[116].A.B. Stoian, M. Vardaki, D. Ionita, M. Enachescu, M. Prodana, O. Brancoveanu, I. Demetrescu, *Nanopores and nanotubes ceramic oxides elaborated on titanium alloy with zirconium by changing anodization potentials*, Ceramics International, Volume 44, Issue 6, pages. 7026–7033, **2018**

[117].T. Kokubo, H. Kushitani, S. Sakka, T. Kitsugi, T. Yamamuro, *Solutions able to reproduce in vivo surface-structure changes in bioactive glass-ceramic A-W*, Journal of Biomedical Materials Research, Volume 24, Issue 6, pages 721–734, **1990**

[119].G.S. El-Sayyad, H.S El-Bastawisy, G. Gobara, A.I. El-Batal, *Gentamicin-Assisted Mycogenic Selenium Nanoparticles Synthesized Under Gamma Irradiation for Robust Reluctance of Resistant Urinary Tract Infection-Causing Pathogens*, Biol. Trace Elem. Res., Volume 195, pages 323–342, **2020**, doi: 10.1007/s12011-019-01842-z

[129].J.E. Gray-Munro, M. Strong, *The mechanism of deposition of calcium phosphate coatings from solution onto magnesium alloy AZ31*, J. Biomed. Mater. Res. Part A, Volume 90A, pages 339–350, **2009**

[130].P. Makkar, S.K. Sarkar, A.R. Padalhin, N.-G. Moon, Y.S. Lee, B.T. Lee, *In vitro and in vivo assessment of biomedical Mg-Ca alloys for bone implant applications*, J. Appl. Biomater. Funct. Mater., Volume 16, pages 126–136, **2018**

[132].R. Ion, A. Mazare, C. Dumitriu, C. Pirvu, P. Schmuki, A. Cimpean, *Nanochannelar topography positively modulates osteo-blast differentiation and inhibits osteoclastogenesis*, Coatings, Volume 8, page 294, **2018**, doi:10.3390/coatings8090294

[133].M.J. Frank, M.S. Walter, S.P. Lyngstadaas, E. Wintermantel, H.J. Haugen, *Hydrogen content in titanium and a titanium–zirconium alloy after acid etching*, Mater. Sci. Eng. C, Volume 33, pages 1282–1288, **2013**, doi:10.1016/j.msec.2012.12.027

[136].Yussuf, A.; Al-Saleh, M.; Al-Enezi, S.; Abraham, G. *Synthesis and characterization of conductive polypyrrole: The influence of the oxidants and monomer on the electrical, thermal, and morphological properties*. Int. J. Polym. Sci. **2018**, 4191747. https://doi.org/10.1155/2018/4191747

[137].R. Batul, M. Bhave, P. Mahon, A. Yu, *Polydopamine Nanosphere with In-Situ Loaded Gentamicin and Its Antimicrobial Activity*, Molecules, Volume 25, 2090, **2020**, doi:10.3390/molecules25092090

[138].B. Rikhari, S.P. Mani, N. Rajendran, *Polypyrrole/graphene oxide composite coating on Ti implants: a promising material for biomedical applications*, J Mater Sci., Volume 55, pages 5211–5229, **2020**

[138].B. Rikhari, S.P. Mani, N. Rajendran, *Polypyrrole/graphene oxide composite coating on Ti implants: a promising material for biomedical applications*, J Mater Sci., Volume 55, pages 5211–5229, **2020**

ANNEX

LIST OF PUBLICATIONS

ISI Indexed Articles

1. *Manuela-Elena VOICU*, Florentina GOLGOVICI, A Biointerface Growth at Immersion of a Biodegradable Magnesium Alloy in Simulated Body Fluid, U.P.B. Scientific Bulletin, Series B: Chemistry and Materials Science, Volume 82, Issue 2, Pages 57−68, 2020, ISSN 1454−2331, WOS:000550842800006, **IF 2022: 0.5**

2. *Manuela Elena VOICU*, Andrei Bogdan STOIAN, Ioana DEMETRESCU, Daniela IONITA, Characterization of Three Surface Treatments on TiZr-Coating Properies and Corrosion Behavior, Coatings, Volume 11, Issue 6, Page 615, 2021, https://doi.org/10.3390/coatings11060615, WOS:000666718100001, **IF 2022: 3.4**

3. *Manuela Elena VOICU*, Ioana DEMETRESCU, Andrei DOROBANTU, Marius ENACHESCU, George-Octavian BUICA, Daniela IONITA, Interaction of Mg Alloy with PLA Electrospun Nanofibers Coating in Understanding Changes of Corrosion, Wettability, and pH, Nanomaterials, Volume 12, Issue 8, Page 1369, 2022, https://doi.org/10.3390/nano12081369, WOS:000785507100001, **IF 2022: 5.3**

4. *Manuela Elena VOICU*, Doina DRAGANESCU, Valentina ANUTA, Andrei Bogdan STOIAN, Daniela IONITA, Ioana DEMETRESCU, The interrelationship between the drug embedded TiZr surface properties and antibacterial effect, Revista Farmacia, Volume 70, Issue 6, Pages 1064−1071, 2022, ISSN 00148237, https://doi.org/10.31925/farmacia.2022.6.9, WOS:000969664100009, **IF 2022: 1.6**

5. *Manuela Elena VOICU*, Florentina GOLGOVICI, Mariana PRODANA, Doina DRAGANESCU, Ioana DEMETRESCU, Advanced procedure of simultaneous electrodeposition from a natural deep eutectic solvent of a drug and a polymer used to improve TiZr alloy behavior, Materials, Volume 16, Issue 12, Page 4387, 2023, https://doi.org/10.3390/ma16124387, WOS:001017534100001, **IF 2022: 3.4**

6. *Manuela Elena VOICU*, Daniela IONITA, George-Octavian BUICA, Doina DRAGANESCU, Valentina ANUTA, Florentina Monica RADULY, Ioana DEMETRESCU, Characterization of two types of polylactic acid coating loaded with gentamicin sulphate deposed on AZ31 alloy, Coatings, Volume 13, Issue 6, Page 1105, 2023, https://doi.org/10.3390/coatings13061105, WOS:001017030800001, **IF 2022: 3.4**

Cumulative Impact factor: 0.5 + 3.4 + 5.3 + 1.6 + 3.4 + 3.4 = 17.6

Conference participation

1. Florentina GOLGOVICI, *Manuela VOICU*, Ioana DEMETRESCU, Electrochemical behavior of magnesium alloy with and without polymeric coatings electrodeposited from ionic liquids, 21st Romanian International Conference on Chemistry and Chemical Engineering, Sept. 4−7, 2019, Constanța, Romania − Poster

2. *Manuela-Elena VOICU*, Daniela IONIȚĂ, Andrei Bogdan STOIAN, Ioana DEMETRESCU, Elaborarea și caracterizarea unui bioaliaj bazat pe TiZr și nanofibre de PLA (Elaboration and characterization of a bioalloy based on TiZr and PLA nanofibers), Conferința națională științifică de toamnă a AOSR, 23−27 noiembrie 2020, Online − Presentation

3. *Manuela Elena VOICU*, Andrei Bogdan STOIAN, Ioana DEMETRESCU, Daniela IONITA, In-Depth characterization of electrospun polylactic acid (PLA) nanofibers on TiZr oxide, International Online Conference, Applications of Chemistry in Nanosciences and Biomaterials Engineering (NanoBioMat 2021), AOSR, June 25−26, 2021, Online − Poster